Published in final edited form as:
*Nat Immunol*. 2017 April ; 18(4): 442–455. doi:10.1038/ni.3694.

# Essential role of the transcription factor Bhlhe41 in regulating the development, self-renewal and BCR repertoire of B-1a cells

**Taras Kreslavsky**[1], **Bojan Vilagos**[1,5], **Hiromi Tagoh**[1,6], **Daniela Kostanova Poliakova**[1], **Tanja Schwickert**[1], **Miriam Wöhner**[1], **Markus Jaritz**[1], **Siegfried Weiss**[2], **Reshma Taneja**[3], **Moritz J. Rossner**[4], and **Meinrad Busslinger**[1]

[1]Research Institute of Molecular Pathology (IMP), Vienna Biocenter (VBC), Campus-Vienna-Biocenter 1, A-1030 Vienna, Austria

[2]Department of Molecular Immunology, Helmholtz Center for Infection Research, Braunschweig, and Institute of Immunology, Medical School, Hannover, Germany

[3]Department of Physiology, Yong Loo Lin School of Medicine, National University of Singapore, Singapore

[4]Department of Psychiatry, Ludwig Maximillian University of Munich, Nussbaumstrasse 7, D-80336 Munich, Germany

## Abstract

Innate-like B-1a cells provide a first line of defense against pathogens, yet little is known about their transcriptional control. Here we identified an essential role of the transcription factor Bhlhe41, with a lesser contribution of Bhlhe40, in controlling late stages of B-1a cell differentiation. *Bhlhe41*$^{-/-}$*Bhlhe40*$^{-/-}$ B-1a cells were severely reduced as compared to their wild-type counterparts. Mutant B-1a cells exhibited an abnormal cell-surface phenotype and altered B-cell receptor (BCR) repertoire exemplified by loss of the phosphatidylcholine-specific $V_H12/V\kappa4$ BCR. Expression of a pre-rearranged $V_H12/V\kappa4$ BCR failed to rescue the mutant phenotype and revealed enhanced proliferation accompanied with increased cell death. Bhlhe41 directly repressed the expression of cell cycle regulators and inhibitors of BCR signaling, while enabling pro-



Correspondence should be addressed to M.B. (busslinger@imp.ac.at).
[5]Present address: Research Center for Molecular Medicine (CeMM), Austrian Academy of Sciences, Lazarettgasse 14, A-1090 Vienna, Austria
[6]Present address: Ludwig Institute for Cancer Research, University of Oxford, Roosevelt Drive, Oxford OX3 7DQ, UK

**Accession Codes**
RNA-seq, ChIP-seq and ATAC-seq data are available at the Gene Expression Omnibus (GEO) repository under the accession numbers GSE93764.

**Author Contributions**
T.K. designed and did most experiments; B.V. discovered Bhlhe41 as a B-1 cell-specific transcription factor; H.T. performed the ATAC-seq experiments; D.K.P. generated the targeted *Bhlhe41*$^{Tag}$ embryonic stem cells; T.S. and M.W. provided advice and help with immunization experiments; M.J. performed the bioinformatics analysis of the ChIP-seq data; S.W. provided PtC-containing liposomes; R.T. and M.J.R. provided the *Bhlhe40* and *Bhlhe41* mutant mice, respectively; T.K and M.B. planned the project and wrote the manuscript.

**Competing Financial Interests**
The authors declare no competing financial interests.

survival cytokine signaling. Thus, Bhlhe41 controls the development, BCR repertoire and self-renewal of B-1a cells.

**Keywords**

Bhlhe41; transcriptional control; B-1a cell development; BCR repertoire; B-1a cell self-renewal; cell cycle regulation; cytokine signaling

## Introduction

B-1 cells are innate-like B lymphocytes1 that provide a first line of defense against pathogens and contribute to tissue homeostasis2,3. They populate the peritoneal and pleural cavities, their associated fat tissue and the spleen. Plasma cells derived from B-1 cells are the major source of IgM antibodies, which are present in an unchallenged organism and are known as “natural antibodies”1. B-1 cells can be distinguished from conventional B cells (referred to as B-2 cells) by their characteristic $B220^{lo}CD19^{+}CD23^{-}CD43^{+}$ phenotype2,3. The major subset of B-1 cells, known as B-1a cells, express the surface marker CD5, while the smaller $CD5^{-}$ fraction is referred to as B-1b cells.

B-1a cells are autoreactive and require a strong B cell receptor (BCR) signal for their differentiation4. Consequently, the differentiation of B-1a cells is impaired by mutations that attenuate BCR signaling or its costimulatory pathways5, whereas the loss of negative regulators of BCR signaling results in an expanded B-1a cell compartment6,7. B-1a cells have a restricted BCR repertoire2,3, which includes BCR specificities that recognize self carbohydrates and lipids8. Notably, a substantial fraction of the murine peritoneal B-1a cells express the $V_H12/V\kappa4$ or $V_H11/V\kappa14(V\kappa9)$ BCR, both of which recognize phosphatidylcholine (PtC)9 that is present in plasma membranes of host cells and in some pathogenic bacteria10.

The first wave of B-1 cell development takes place during fetal and neonatal life and largely contributes to the adult B-1 cell compartment, as B-1 cells can self-renew throughout the lifetime of the organism3,11,12. By contrast, conventional follicular (FO) and marginal zone (MZ) B-2 cells are constantly replenished by differentiation from hematopoietic stem cells (HSCs) in the bone marrow. Adult HSCs also contribute to B-1 cell differentiation13–15, although to a lower extent compared to fetal hematopoiesis12. The development of B-1 cells is still poorly understood and explained by two models. According to the “lineage model”, B-1 and B-2 cells develop along distinct B cell lineages prior to BCR expression3,16, which is supported by the identification of a B-1-specified progenitor cell population ($Lin^{-}CD93^{+}CD19^{+}B220^{-/lo}$) that preferentially gives rise to B-1 cells17,18. The “selection model” proposes that the B-1a cell fate decision occurs after IgM expression by antigen-driven selection of a B-1a cell-specific BCR4,19–21.

Due to their unique physiological properties, innate-like B-1 cells are likely controlled by a transcriptional program that differs from that of B-2 cells. Indeed, the transcription factor Arid3a was implicated in controlling B-1 cell development by acting in the Lin28b–Let7–Arid3a pathway22,23. Moreover, loss of the pan-B cell regulators Oct2 (ref. 24) or IκBNS25




Europe PMC Funders Author Manuscripts

more severely affect B-1 cell generation than B-2 cell development. However, our understanding of the transcriptional network controlling B-1 cell identity and function remains rudimentary.

Here we report that B-1a cells depend on the basic-helix-loop-helix (bHLH) transcription factors Bhlhe41 and Bhlhe40, which are known to regulate different physiological processes in non-immune cells26,27 and to control immune responses in T cells28–30. *Bhlhe41* was highly expressed only in B-1 cells, whereas its closest homolog, *Bhlhe40*, was lowly and broadly expressed in the B-lymphoid lineage. B-1a cell numbers were strongly reduced in *Bhlhe41*$^{-/-}$ mice, and this phenotype was more severe in *Bhlhe41*$^{-/-}$*Bhlhe40*$^{-/-}$ mice. Detailed analysis of the double-knockout (DKO) B-1a cells demonstrated a major role of Bhlhe41, with a lesser contribution of Bhlhe40, in controlling multiple aspects of B-1a cell biology, including their development, life-long self-renewal, unique cell surface phenotype and restricted BCR repertoire.

## Results

### B-1 cell-specific expression of *Bhlhe41*

By analyzing the gene expression differences between murine splenic B-1a and FO B cells, we identified *Bhlhe41* (also known as *Dec2* or *Sharp1*) as a gene that exhibited a 23-fold higher expression in B-1a cells compared to FO B cells31 (Supplementary Fig. 1a). Within the hematopoietic system, *Bhlhe41* was highly expressed only in B-1a and B-1b lymphocytes, lung macrophages and microglia32 (Supplementary Fig. 1b). During B cell development, *Bhlhe41* was lowly expressed in pre-B, immature B and plasma cells of the bone marrow and in transitional B cells of the spleen (Supplementary Fig. 1b,c). As Bhlhe40 (also known as Dec1, Sharp2 or Stra13) is a close homolog of Bhlhe41 and both transcription factors have often redundant functions33,34, we also assessed *Bhlhe40* expression. *Bhlhe40* exhibited a broad pattern of low expression in B cells compared to its high expression in myeloid, NK and T cells (Supplementary Fig. 1b,c).

To analyze *Bhlhe41* expression at the single-cell level, we generated a BAC transgenic mouse line expressing an iCre-IRES-hCD2 gene cassette under the control of *Bhlhe41* regulatory elements. The hCD2 reporter was highly expressed by all B-1 cells (Fig. 1a). Low hCD2 expression was detected on MZ B cells, plasma cells and transitional B cells in the spleen. Pre-B, immature and transitional B cells in the bone marrow exhibited only very low hCD2 expression, while pro-B, FO B, T and NK cells were largely hCD2-negative (Fig. 1a and Supplementary Fig. 1d). *Bhlhe41* was, however, more highly expressed in immature B cells of the fetal and neonatal liver compared to their adult bone marrow counterparts (Supplementary Fig. 1b,e), which correlates with the higher propensity of fetal and neonatal precursors to generate B-1 cells3.

### *Bhlhe41* is induced in follicular B cells upon activation

As the transcriptional programs of innate-like lymphocytes and their activated conventional counterparts often overlap, we interrogated RNA-seq datasets of lipopolysaccharide (LPS)-stimulated FO B cells for *Bhlhe41* expression35. *Bhlhe41* expression was strongly induced

Europe PMC Funders Author Manuscripts

upon LPS stimulation (Supplementary Fig. 1f), while *Bhlhe40* was downregulated, as reported36. Stimulation of sorted FO B cells from *Bhlhe41*-Cre-hCD2 reporter mice with LPS, anti-IgM plus IL-4 or anti-CD40 plus IL-4 furthermore revealed that the *Bhlhe41* reporter was induced under all three conditions (Supplementary Fig. 1g). We therefore speculate that *Bhlhe41* may be upregulated during B-1 cell development as a result of the self-reactivity of B-1 cells.

## B-1a cells are dependent on Bhlhe41

To investigate the role of Bhlhe41 in B lymphopoiesis, we compared the B cell developmental stages and mature B cell subsets in wild-type and *Bhlhe41*$^{-/-}$ mice as well as in *Bhlhe40*$^{-/-}$*Bhlhe41*$^{-/-}$ mice, since Bhlhe41 often functions redundantly with Bhlhe40 (ref. 33,34). B cell development in the fetal liver and bone marrow was unaffected (Supplementary Fig. 2a–c), and the numbers of splenic MZ and FO B cells were also unchanged in the single- and double-mutant mice (Fig. 1b and Supplementary Fig. 2d). Moreover, the DKO B cells produced NP-specific antibodies upon NP-KLH immunization similar to wild-type B cells (data not shown). We conclude therefore that neither B-2 cell development nor immune responses are grossly affected by the Bhlhe41/Bhlhe40 deficiency.

*Bhlhe41*$^{-/-}$ mice exhibited, however, a severe reduction in B-1a cell numbers in the spleen and peritoneal cavity, and the DKO mice showed a slight further reduction of B-1a cells (Fig. 1b-e). B-1a cells were, however, not decreased in *Bhlhe40*$^{-/-}$ mice (Supplementary Fig. 2e). The residual DKO B-1a cells exhibited an altered surface phenotype, as indicated by lower expression of CD5 and higher expression of B220 (Fig. 1c). Although B-1b cells also highly express *Bhlhe41* (Fig. 1a and Supplementary Fig. 1b,c), there were not decreased in the knockout mice (Fig. 1c and Supplementary Fig. 2d). Together, these data identified an essential role for Bhlhe41 in the generation of B-1a cells, while Bhlhe40 contributed to this process to a lesser extent, consistent with its low expression in B-1a cells (Supplementary Fig. 1b,c).

We next analyzed mixed fetal liver chimeras generated by transfer of a 1:1 mixture of wild-type (WT; CD45.1) and DKO (CD45.2) E14.5 fetal liver cells into lethally irradiated *Rag2*$^{-/-}$ mice. The WT-to-DKO ratio in pro-B, pre-B and B cells of the bone marrow, total splenic B-2 cells and peritoneal B-2 and B-1b cells closely reflected that of the LSK stem/progenitor cell compartment, thus confirming that Bhlhe41 and Bhlhe40 are dispensable for B-2 cell development and homeostasis (Fig. 1f,g). In contrast, B-1a cells of the chimeras originated predominantly from wild-type precursors (Fig. 1f,g). Similar results were obtained when bone marrow rather than fetal liver cells were used to generate chimeras, although the competitive disadvantage of the bone marrow DKO cells was reduced (Supplementary Fig. 2f), indicating that fetal liver-derived B-1a cells may be more sensitive to the loss of Bhlhe41 and Bhlhe40. Together these experiments identified Bhlhe41 and Bhlhe40 as cell-intrinsic regulators of B-1a cell differentiation and/or homeostasis.

## Altered BCR repertoire of *Bhlhe41*$^{-/-}$*Bhlhe40*$^{-/-}$ B-1a cells

We next compared the gene expression of the residual DKO B-1a cells with their wild-type counterparts by RNA-seq. As shown by principal component analysis (PCA), the DKO B-1a

cells clustered closely with their wild-type counterparts away from FO and MZ B cells (Supplementary Fig. 3a), indicating that these cells largely maintained their B-1a cell identity. Unexpectedly, the most prominent group of differentially expressed genes encoded V segments of the immunoglobulin heavy- and light-chains (Fig. 2a,b), indicating that the BCR repertoire of the DKO B-1a cells was drastically altered. The most differentially expressed V gene segments corresponded to *Ighv12-3* and *Igkv4-91*, which were almost completely absent from the BCR repertoire of DKO B-1a cells (Fig. 2a,b). The $V_H12$ and Vκ4 chains constitute a phosphatidylcholine (PtC)-specific BCR9 that is expressed by ~10% of peritoneal B-1 cells (Fig. 2c,d). Staining with an anti-$V_H12$ antibody or fluorochrome-loaded PtC-containing liposomes confirmed a drastic decrease in $V_H12^+$ and PtC-specific B-1a cells in *Bhlhe41*$^{-/-}$ mice and an almost complete loss of $V_H12^+$ cells in DKO mice (Fig. 2c,d). The few residual PtC-specific cells likely express the Vh11/Vk14 BCR, as *Ighv11*-2 and *Igkv14-126* transcripts were detectable in DKO B-1a cells (Fig. 2b). The 'missing' $V_H12$ and Vκ4 segments did not reappear in the $CD5^-$ B-1b cell fraction (Fig. 2b,c), excluding the possibility that the PtC-specific cells merely lost CD5 expression. Analysis of fetal liver (Fig. 1f,g) and bone marrow (Supplementary Fig. 2f) chimeras confirmed that the loss of $V_H12^+$ B-1 cells in DKO mice was cell-intrinsic. Hence, Bhlhe41 together with Bhlhe40 is responsible for sculpting the BCR repertoire of B-1a cells.

## Control of B-1a cell development by Bhlhe41 and Bhlhe40

To investigate a role of Bhlhe41 in B-1a cell development, we assessed the expression of *Bhlhe41* and the consequence of Bhlhe41/Bhlhe40 deficiency in the B-1-specified progenitors, which can be identified as a BCR-negative $Lin^-CD93^+CD19^+B220^{-/lo}$ cell population at fetal, neonatal and adult sites of hematopoiesis17. No expression of the *Bhlhe41*-iCre-IRES-hCD2 reporter gene was observed in these progenitors in the fetal and neonatal liver, neonatal and adult bone marrow, and neonatal spleen (Fig. 3a and Supplementary Fig. 3b). Moreover, the frequency of the B-1-specified progenitors was not affected by the absence of Bhlhe41 and Bhlhe40 (Fig. 3a). We next examined the expression and function of Bhlhe41 in the $CD93^+IgM^+CD19^+B220^{lo}CD5^+$ transitional B-1a (TrB-1a) cells that can be detected in the spleen one week after birth25. This population highly expressed the *Bhlhe41*-iCre-IRES-hCD2 reporter gene in wild-type mice and was largely lost in *Bhlhe41*/*Bhlhe40* DKO mice (Fig. 3b). Hence, Bhlhe41 and Bhlhe40 are required for the generation of transitional B-1a cells.

We next tested whether the BCR repertoire alterations observed in adult DKO mice may arise from a defect in an early selection event or a later failure of these cells to expand. To this end, we characterized the emergence of $V_H12^+$ PtC-specific B-1a cells early in the ontogeny of wild-type mice. While very low numbers of $V_H12^+$ B cells could be detected in day-1 neonatal liver, these cells were not PtC-specific as judged by the lack of PtC liposome binding (Fig. 3c). Small numbers of both $V_H12^+$ and $V_H12^-$ PtC-specific cells could, however, be detected in splenocytes at postnatal day 9 (Fig. 3d and Supplementary Fig. 3c). The PtC-specific cells were thus scarce in neonates and only expanded in adult mice (Fig. 3d and Supplementary Fig. 3c), consistent with the notion that $V_H12^+$ B-1a cells pass through several selection bottlenecks during their development9,13. We next investigated the effect of Bhlhe41/Bhlhe40 deficiency on $V_H12^+$ B cells at different stages of ontogeny.

Comparable numbers of non-PtC-specific $V_H12^+$ B cells were present in wild-type and DKO neonatal livers at day 1 (Fig. 3c), indicating that Bhlhe41 and Bhlhe40 were dispensable for $V_H$-$DJ_H$ recombination of the $V_H12$ gene segment. The emergence of PtC-specific $V_H12^+$ cells later in neonatal spleens at day 9 was, however, severely compromised in DKO mice, whereas the non-PtC-specific $V_H12^+$ B cells were not affected (Fig. 3d). Hence, Bhlhe41 and Bhlhe40 control the earliest stages of B-1a BCR repertoire selection but not *Igh* rearrangements consistent with the lack of their expression in pro-B cells.

## No rescue of the DKO phenotype by $V_H12$ and Vκ4 transgenes

As the phenotype and gene expression pattern of DKO B-1a cells may be indirectly affected by the altered BCR repertoire, we generated DKO mice expressing pre-rearranged $V_H12$ and Vκ4 transgenes37 that encode the two immunoglobulin chains, which are largely missing from the BCR repertoire of DKO B-1a cells. The $V_H12$ transgene alone or together with the Vκ4 transgene diverted most of the developing B cells towards the B-1a cell fate37, as virtually all B cells in the peritoneal cavities of both $V_H12$ and $V_H12$/Vκ4 transgenic mice on a wild-type background were $V_H12^+$ and had the $CD5^{hi}CD23^{-}B220^{lo}CD19^+$ B-1a cell phenotype (Fig. 4a and Supplementary Fig. 4a). As shown by principal component analysis of RNA-seq data, these $V_H12$/Vκ4 transgenic B-1a cells clustered closely together with polyclonal B-1a cells (Supplementary Fig. 4b), demonstrating that expression of the $V_H12$ and Vκ4 transgenes promoted the generation of largely normal B-1a cells. The $V_H12$/Vκ4 transgenic B-1a cells on the DKO background had, however, a severely altered cell surface phenotype similar to that of non-transgenic DKO B-1a cells, as they failed to downregulate B220, were $CD5^{int}$ and contained a sizable fraction of $CD23^+$ cells (Fig. 4a,b and Supplementary Fig. 4a). Hence, the aberrant cell surface phenotype of DKO B-1a cells is not a result of the altered BCR repertoire.

The peritoneal B-1a cells of $V_H12$-only transgenic DKO mice were severely reduced (Fig. 4c) like the B-1a cells of non-transgenic DKO mice. In contrast, the frequencies of peritoneal B-1a cells in $V_H12$/Vκ4 double-transgenic DKO and wild-type mice were similar (Fig. 4c). One possible explanation for this discrepancy could be that the strong overproduction of B-1a cells in the $V_H12$/Vκ4 transgenic mice, even on the DKO background, may mask the phenotype. Indeed, the additional expression of the Vκ4 transgene in $V_H12$ transgenic wild-type mice increased the frequency of $V_H12^+$ cells in the bone marrow approximately 8-fold (Supplementary Fig. 4c). To decrease the B-1a cell output, we reduced the frequency of BCR transgenic precursors by generating chimeric mice, in which B cell-depleted bone marrow from $CD45.2^+$ $V_H12$/Vκ4 transgenic mice, either on a wild-type or DKO background, was “diluted” 1:9 with bone marrow from non-transgenic wild-type $CD45.1^+$ mice. In this transplantation setting (referred to “10% chimeras”), the contribution of the $V_H12$/Vκ4 transgenic wild-type or DKO bone marrow to the LSK cell compartment was close to 10%, as expected (Fig. 4d). In the peritoneal cavity, however, $V_H12$/Vκ4 transgenic DKO B-1a cells were decreased 5.5-fold compared to their BCR-transgenic wild-type counterparts (Fig. 4d). Therefore, the generation and/or self-renewal of DKO B-1a cells was impaired in polyclonal, $V_H12$ transgenic and $V_H12$/Vκ4 double-transgenic mice.

We conclude that expression of the pre-rearranged $V_H12$ and Vκ4 transgenes rescued neither the qualitative (surface phenotype) nor quantitative (cell number) phenotype of DKO B-1a cells. Importantly, the $V_H12$/Vκ4 transgenic system provided us with a comparable setting for investigating the cellular and molecular mechanisms causing the observed phenotype, as it eliminated potential confounding effects of the altered BCR repertoire in the DKO mice.

## Bhlhe41 functions as a transcriptional repressor

We next investigated the molecular function of Bhlhe41 by identifying regulated Bhlhe41 target genes in B-1a cells by ChIP-seq and RNA-seq analyses. To this end, we generated a *Bhlhe41* knock-in allele (*Bhlhe41*$^{Tag}$) by inserting at the last Bhlhe41 codon a sequence encoding multiple tags including the V5 epitope (Supplementary Fig. 5a). Notably, the B-1a cell compartment was indistinguishable in *Bhlhe41*$^{Tag/Tag}$ and wild-type mice (Supplementary Fig 5b), indicating that the inserted tag sequences did not interfere with Bhlhe41 function. We next used splenic B-1a cells of $V_H12$/Vκ4 transgenic *Bhlhe41*$^{Tag/Tag}$ to obtain sufficient cell numbers for ChIP-seq analysis with an anti-V5 antibody. Peak calling with a stringent *P* value of $< 10^{-10}$ identified 5,757 Bhlhe41-binding regions, which defined 5,509 Bhlhe41 target genes in B-1a cells (data not shown). Analysis of the Bhlhe41 peak sequences with *de novo* motif-discovery programs identified the E-box motif CACGTG (Fig. 5a) that closely resembles the previously identified Bhlhe41- and Bhlhe40-binding motifs38. Notably, most Bhlhe41 peaks were located at gene promoters (63%; Fig. 5b) and present in open chromatin regions (Fig. 5c,d), which were determined by the assay for transposase-accessible chromatin (ATAC) combined with deep sequencing (ATAC-seq)39.

To identify genes regulated by Bhlhe41 and Bhlhe40, we compared $V_H12$/Vκ4 transgenic wild-type and DKO B-1a cells by RNA-seq. This analysis identified 168 activated and 151 repressed genes (Fig. 5e), which were selected for an expression difference of > 2-fold, an adjusted *P* value of < 0.05 and a TPM value (transcripts per million) of > 5 in one of the two cell populations. As RNA-seq was also performed with non-transgenic wild-type and DKO B-1a cells, we compared both RNA-seq datasets by gene set enrichment analysis (GSEA), which revealed similar gene regulation by Bhlhe41 and Bhlhe40 in $V_H12$/Vκ4 transgenic and polyclonal B-1a cells (Supplementary Fig. 5c). By determining the overlap between the Bhlhe41-bound genes and Bhlhe41-regulated genes, we identified 41 potentially directly activated and 90 potentially directly repressed target genes (Fig. 5d,e). Importantly, the majority (60%) of repressed genes were bound by Bhlhe41 in contrast to only 24% of the activated genes (Fig. 5e), which strongly suggests that Bhlhe41 predominantly functions as a transcriptional repressor in B-1a cells. As shown by ATAC-seq, Bhlhe41-mediated repression was not associated with a decrease in chromatin accessibility (Supplementary Fig. 5d).

## Impaired BCR signaling in $V_H12$/Vκ4 transgenic DKO B-1a cells

As B-1a cells depend on strong BCR signaling4,5, we next compared the phosphorylation of BCR signaling components in wild-type and DKO B-1a cells. Consistent with constitutive BCR signaling in B-1a cells40,41, we noticed that the phosphorylation of BCR signaling

components could be readily detected in *ex vivo* B-1a cells without exogenous stimulation, when the cells were kept on ice prior to fixation. Our analysis did not reveal any reproducible signaling defects in polyclonal DKO B-1a cells (data not shown), possibly due to the selection of BCRs that undergo normal BCR signaling in the absence of Bhlhe41 and Bhlhe40. In contrast, BCR signaling was impaired in $V_H12/V\kappa4$ transgenic DKO B-1a cells, which exhibited decreased phosphorylation of BLNK, Btk, ERK, PLC$\gamma$2, and Syk compared to $V_H12/V\kappa4$ transgenic wild-type B-1a cells (Fig. 6a). The $V_H12/V\kappa4$ transgenic DKO B-1a cells were, however, not anergic, as they show normal intracellular calcium signaling upon anti-IgM stimulation of the BCR (Supplementary Fig. 6a).

Most genes coding for core components of BCR signaling were similarly expressed in $V_H12/V\kappa4$ transgenic wild-type and DKO B-1a cells except for two gene classes (Supplementary Fig. 6b). First, the *Ighm* transcript, encoding the constant region of the immunoglobulin μ-heavy chain, was 1.7-fold reduced in $V_H12/V\kappa4$ transgenic DKO B-1a cells compared to their wild-type counterparts, which resulted in a corresponding decrease in surface IgM expression (Supplementary Fig. 6c). Co-staining for intracellular IgM and phosphorylated epitopes of signal transducers demonstrated a correlation between the expression of the $V_H12/V\kappa4$ BCR and phosphorylation of BCR signaling components (Supplementary Fig. 6d), indicating that a mild decrease in IgM expression in DKO cells could have functional consequences. IgM (*Ighm*) expression was, however, not reduced in polyclonal DKO B-1a cells (data not shown), possibly due to selection of the altered BCR repertoire of these cells. Second, the expression of several negative regulators of BCR signaling was derepressed in both $V_H12/V\kappa4$ transgenic and polyclonal DKO B-1a cells (Fig. 6b). This included *Lpxn*, encoding an inhibitory adaptor protein42, and *Cd72*, encoding an ITIM-containing receptor known to restrict B-1 cell numbers7. Surface expression of CD72 was also increased both on polyclonal and $V_H12/V\kappa4$ transgenic DKO B-1a cells (Fig. 6c), which could restrict B-1a cell accumulation, as reported7. Four genes (*Dusp1, Dusp2, Dusp4,* and *Dusp6*), encoding dual specificity phosphatases that can dephosphorylate ERK, JNK and p38, were also derepressed in the absence of Bhlhe41 and Bhlhe40 (Fig. 6b). Importantly, all six genes were directly repressed by Bhlhe41 as shown by the presence of Bhlhe41-binding sites in their vicinity (Figs. 5d and 6d). Hence, the BCR signaling defects in $V_H12/V\kappa4$ transgenic DKO B-1a cells were associated with derepression of several negative regulators of this pathway.

As PtC-specific $V_H12/V\kappa4$-positive B-1a cells are lost in DKO mice, we next investigated whether these B-1a cells are particularly sensitive to defective BCR signaling. To this end, we analyzed PtC-specific B-1a cells in $Cd19^{-/-}$ mice that have drastically decreased B-1a cell numbers due to lack of the co-stimulatory receptor CD1943. While the residual B-1a cells still contained some PtC-specific cells in the peritoneal cavity of $Cd19^{-/-}$ mice, the $V_H12^+$ cells were strongly decreased (Fig. 6e and Supplementary Fig. 6e) similar to *Bhlhe41/Bhlhe40* mutant mice. Hence, the $V_H12/V\kappa4$-positive B-1a cells seem to be particularly sensitive to impaired BCR signaling.




Europe PMC Funders Author Manuscripts

### Bhlhe41 and Bhlhe40 restrict B-1a cell proliferation

As B-1a cell numbers were severely decreased in DKO mice, we investigated whether proliferation was affected by loss of Bhlhe41 and Bhlhe40. Most wild-type and $V_H12/V\kappa4$ transgenic B-1a cells exhibited low expression of the proliferation marker Ki67 (Fig. 7a-c), consistent with their slow proliferation in steady state. Unexpectedly, DKO B-1a cells both in the polyclonal and $V_H12/V\kappa4$ transgenic settings exhibited a 3-fold increase in $Ki67^{hi}$ cells and in cells present at the S, G2 or M phase of the cell cycle (Fig. 7a-c). Moreover, the same phenotype was evident in mixed fetal liver chimeras generated with non-transgenic wild-type and DKO cells (Fig. 7d). Hence, the increased proliferation is a cell-autonomous property of the DKO B-1a cells.

Several genes encoding known or putative cell cycle regulators were identified a repressed Bhlhe41 target genes, as they were more highly expressed in DKO B-1a cells and were bound by Bhlhe41 in wild-type B-1a cells (Fig. 7e,f and Supplementary Fig. 7a,b). Six of these genes code for cyclin H (*Ccnh*), a cyclin-dependent kinase-like protein (*Cdkl1*), a regulatory subunit (*Cks2*) of cyclin-dependent kinases, two helicases (*Hells*, *Recql5*) implicated in DNA replication and a deubiquitinase (*Usp28*) involved in the G2 DNA damage checkpoint (Supplementary Fig. 7a,b). Notably, the expression of 4 (*E2f1*, *E2f2*, *E2f7*, *E2f8*) of 8 genes coding for members of the cell cycle-regulating E2F transcription factor family was also increased in DKO cells (Fig. 7e), and Bhlhe41 binding was observed at *E2f1*, *E2f7* and *E2f8* (Fig. 5d and Fig. 7f), suggesting that they are directly repressed by Bhlhe41. If Bhlhe41 and Bhlhe40 restrict B-1a cell proliferation by downregulating the expression of E2F transcription factors, E2F target genes should likewise be upregulated in DKO B-1a cells. Indeed, gene set enrichment analysis (GSEA) revealed a marked derepression of E2F target genes in DKO B-1a cells compared to wild-type B-1a cells (Fig. 7g). We conclude therefore that Bhlhe41 together with Bhlhe40 enforces slow proliferation of B-1a lymphocytes, at least in part by direct repression of cell cycle regulators including E2F transcription factors.

### Bhlhe41 and Bhlhe40 regulate the self-renewal of B-1a cell

As DKO B-1a cells exhibited increased proliferation despite their decrease in cell numbers, we next investigated whether a defect in survival may contribute to this phenotype. Indeed, *ex vivo* analysis of $V_H12/V\kappa4$ transgenic DKO B-1a cells revealed a 4-fold increase in cell death (Fig. 8a). A similar increase in cell death was, however, not evident in non-transgenic DKO mice (data not shown), possibly due to the selection of cells with reduced sensitivity to the Bhlhe41/Bhlhe40 deficiency. To test if homeostasis of the polyclonal B-1a cells may nevertheless be affected by the loss of Bhlhe41 and Bhlhe40, we sorted peritoneal B-1a cells from wild-type or DKO mice (CD45.2) and transferred them intraperitoneally into sublethally irradiated wild-type recipients (CD45.1). The DKO B-1a cells failed to maintain their numbers and disappeared with relatively slow kinetics after two months from the recipients in contrast to the wild-type B-1a cells (Fig. 8b). In line with this failure to self-renew, peritoneal DKO B-1a cells did not accumulate with age, as their absolute cell numbers remained virtually unchanged between 1 and 4 months, while wild-type B-1a cells significantly increased (Fig. 8c). Consistent with the inability to generate PtC-specific $V_H12^+$ B-1a cells in early ontogeny, a strong decrease of $V_H12^+$ B-1a cells was also evident

in young DKO mice (Fig. 8d). Together, these results indicate that Bhlhe41 and Bhlhe40 regulate the self-renewal of B-1a cells.

We next interrogated our RNA-seq data for possible mediators of the pro-survival function of Bhlhe41 and Bhlhe40. *Tnfrsf13b* (TACI) and *Tnfrsf13c* (BAFF-R) coding for receptors signaling B cell survival were similarly expressed in wild-type and DKO B-1a cells (Supplementary Fig. 8a). In contrast, *Il5ra* transcripts and surface IL-5Rα expression were strongly reduced both in $V_H12/V\kappa4$ transgenic and polyclonal DKO B-1a cells in a cell-intrinsic manner (Fig. 8e,f and Supplementary Fig. 8b). B-1a cells are known to depend on IL-5 receptor signaling, as their cell numbers are decreased in *Il5ra* mutant mice44,45, albeit to a lower extent than in *Bhlhe41/Bhlhe40* mutant mice. We next incubated sorted $V_H12/V\kappa4$ transgenic or polyclonal B-1a cells with or without IL-5. While IL-5 enhanced the survival of wild-type B-1a lymphocytes *in vitro*, it had no effect on DKO B-1a cells (Fig. 8g). We conclude therefore that the residual IL-5 receptor expression is insufficient to mediate the pro-survival function of IL-5 in DKO B-1a cells.

The IL-5 receptor belongs to the family of IL-3, IL-5 and GM-CSF receptors that share the same β-chain (encoded by *Csf2rb*) except for the IL-3 receptor, which can also utilize a related β-chain (encoded by *Csf2rb2*). Notably, the expression of four (*Il5ra, Il3ra*, *Csf2rb, Csf2rb2*) of these five genes was downregulated in DKO B-1a cells (Fig. 8e), which was confirmed by the observed decrease in surface IL-3Rα expression on these cells (Fig. 8f and Supplementary Fig. 8b). No Bhlhe41 binding was detected in the vicinity of these four activated genes (data not shown), which is consistent with a primary role of Bhlhe41 in transcriptional repression. Notably, *Csf2rb/Csf2rb2* double-mutant mice, which are unable to respond to IL-5, IL-3 or GM-CSF46, exhibited a decrease in B-1a cell numbers that was, however, weaker than that observed in *Bhlhe41/Bhlhe40* mutant mice (Fig. 8h). The Csf2rb/Csf2rb2 deficiency did, however, not affect the frequency of $V_H12^+$ B-1a cells in contrast to the Bhlhe41/Bhlhe40 deficiency (Fig. 8h). Moreover, the *Csf2rb/Csf2rb2* mutant phenotype was evident only in older mice (data not shown), consistent with a self-renewal defect. These data therefore demonstrate that Bhlhe41 and Bhlhe40 control the self-renewal of B-1a cells in part by rendering B-1a cells receptive to pro-survival cytokine signaling.

## Discussion

Here we have identified an essential role of the transcription factor Bhlhe41, with a lesser contribution of Bhlhe40, in the control of several key aspects of B-1a cell biology. First, we identified the transitional B-1a cells25 in the neonatal spleen as the earliest developmental stage exhibiting high *Bhlhe41* expression. Consistent with this finding, these transitional B-1a cells were largely lost in the absence of Bhlhe41 and Bhlhe40, indicating that these transcription factors are required for B-1a cell development. Second, while wild-type B-1a cells have a restricted BCR repertoire with several dominant specificities, the DKO B-1a cells had a drastically altered V segment usage, demonstrating that Bhlhe41 together with Bhlhe40 shapes the BCR repertoire of B-1a cells. Finally, in contrast to wild-type B-1a cells, which are capable of life-long survival accompanied by slow proliferation, DKO B-1a cells were decreased in numbers, exhibited aberrantly enhanced proliferation combined with

increased cell death and failed to accumulate with age, indicating that Bhlhe41 and Bhlhe40 control the self-renewal of B-1a cells.

The altered BCR repertoire of DKO B-1a cells suggested that the residual cells were selected for reduced sensitivity to the Bhlhe41/Bhlhe40 deficiency, which could mask some aspects of the mutant phenotype of DKO cells. To avoid such confounding effects, we assessed the DKO phenotype in both polyclonal and $V_H12/V\kappa4$ transgenic B-1a cells. Most aspects of the mutant phenotype were apparent in both settings. This included a severe decrease of B-1a cells, an altered cell surface phenotype, increased cell proliferation, upregulated expression of positive cell cycle regulators, augmented expression of negative regulators of BCR signaling and downregulation of the IL-5 and IL-3 receptors in both DKO B-1a cell types. While a survival defect was more obvious for $V_H12/V\kappa4$ transgenic DKO B-1a cells, polyclonal DKO B-1a cells failed to accumulate with age and, unlike their wild-type counterparts, disappeared upon transfer from the recipients. Given the increased proliferation of DKO cells, these observations point to a survival defect, albeit less acute than that observed in $V_H12/V\kappa4$ transgenic DKO mice. However, one aspect of the DKO phenotype – defective BCR signaling – was only evident in $V_H12/V\kappa4$ transgenic B-1a cells. One possible explanation for this discrepancy could be that the DKO B-1a cells expressing BCR specificities with reduced signaling potential undergo cell death and thus counter-selection during postnatal development, which results in viable DKO B-1a cells with normal BCR signaling in the adult mice analyzed. In contrast, $V_H12/V\kappa4$ transgenic B-1a cells with their attenuated BCR signaling appear to be constantly generated during adult life47 and are thus present at the time of analysis.

The PtC-specific $V_H12/V\kappa4$ BCR is almost completely lost from the repertoire of DKO B-1a cells, possibly due to its impaired signaling in the absence Bhlhe41 and Bhlh40. Here we demonstrated that the $V_H12/V\kappa4$-expressing B-1a cells are particularly sensitive to defective BCR signaling as evidenced by their loss from the BCR repertoire of *Cd19* mutant mice. Notably, mice deficient for the signal transducer RasGRP1 also have a selective decrease in PtC-specific B-1a cells48. While Bhlhe41 does not regulate *Cd19* or *Rasgrp1*, it directly represses multiple genes coding for negative regulators of BCR signaling, including several dual specificity phosphatases and the ITIM-containing receptor CD72, which is known to restrict B-1 cell numbers7. The increased expression of these negative regulators in $V_H12/V\kappa4$ transgenic DKO B-1a cells may contribute to the observed decrease in phosphorylation of BCR signal transducers. This signaling defect likely contributes to both the general decrease of B-1a cell numbers and the selective loss of B-1a cells with certain BCR specificities.

Signaling of the IL-5 receptor was previously implicated in the self-renewal of B-1a cells44,45. Here we have demonstrated that Bhlhe41 and Bhlhe40 are required for expression of both α-chains (*Il5ra*, *Il3ra*) and β-chains (*Csf2rb*, *Csf2rb2*) of the IL-5, IL-3 and GM-CSF-receptor family. While the IL-5Rα expression was 5-fold reduced in DKO B-1a cells compared to wild-type B-1a cells, this low expression was insufficient to mediate pro-survival even when high IL-5 concentrations were used for *in vitro* culture. Moreover, B-1a cells were decreased in *Csf2rb/Csf2rb2* mutant mice, thus providing additional *in vivo* evidence for a functional role of these receptors in B-1a cells. A decrease in B-1a cell

numbers was only obvious in older *Csf2rb*/*Csf2rb2* mutant mice, indicating a role of these receptors in B-1a cell self-renewal in agreement with the age dependency of the respective *Bhlhe41*/*Bhlhe40* mutant phenotype.

B-1a cells, like adult tissue stem cells, undergo self-renewal associated with slow cell proliferation. Consistent with the previous characterization of Bhlhe40 as a cytostatic factor upon overexpression in B cells36,49, we have now identified Bhlhe41 and Bhlhe40 as negative regulators of the cell cycle, as DKO B-1a cells were more proliferative than their wild-type counterparts. Mechanistically, this is likely explained by direct Bhlhe41-mediated repression of multiple genes coding for components of the cell cycle machinery, including three E2F transcription factors. Paradoxically, the accelerated proliferation of the DKO B-1a cells was associated with increased cell death. It is tempting to speculate that the increase in apoptosis may be in part a consequence of the unleashed proliferation, as ectopic activation of the cell cycle machinery can be a potent inducer of cell death50.

The different aspects of the *Bhlhe41/Bhlhe40* mutant phenotype are likely caused by distinct mechanisms. First, while the impaired self-renewal of DKO B-1a cells became more apparent with age, the preferential loss of $V_H12^+$ B-1a cells was observed already in the neonatal spleen of DKO mice. Hence, the self-renewal defect must be independent of the BCR repertoire change. Second, the reduced expression of IL-5 and IL-3 receptors unlikely results from impaired BCR signaling, as the residual B-1a cells in CD19-deficient mice exhibited normal IL-5α expression (data not shown). Finally, the increased proliferation of DKO B-1a cells points to yet another aspect of the Bhlhe41-regulated molecular program, as Bhlhe41 directly represses genes coding for positive cell cycle regulators. Thus, the increased proliferation of DKO B-1a cells seems to be independent of both the reduced BCR signaling and impaired cytokine receptor expression. Bhlhe41 thus executes pleiotropic functions in B-1a cells by controlling distinct aspects of B-1a cell physiology.

## Online Methods

### Mice

The *Bhlhe41*$^{-/-}$ mice51, *Bhlhe40*$^{-/-}$ mice28, *Csf2rb*$^{-/-}$ *Csf2rb2*$^{-/-}$ mice46, *Cd19*$^{-/-}$ mice43, $V_H12$ transgenic line 6-1 (ref. 37) and the Vκ4 transgenic line 1-2 (ref. 37) were described previously. All animal experiments were carried out according to valid project licenses, which were approved and regularly controlled by the Austrian Veterinary Authorities.

### Generation of the transgenic *Bhlhe41*-iCre-IRES-hCd2 mouse

The *Bhlhe41*-Cre-hCD2 reporter mouse was generated as described previously52. In brief, the iCre-IRES-hCD2 gene expression cassette was inserted into the mouse *Bhlhe41* BAC (RP23-343I17) by recombineering in *Escherichia coli*. Transgenic mice were generated by injection of supercoiled BAC DNA into pronuclei of C57BL/6xCBA F1 zygotes.

### Generation of the *Bhlhe41*$^{Tag}$ allele

The *Bhlhe41*$^{Tag}$ allele (Supplementary Fig. 5a) was generated by homologous recombination in mouse ES cells. The corresponding targeting vector was obtained by insertion of the

following sequences in the 5′ to 3′ direction into the *Bhlhe41* bacterial artificial chromosome (BAC) RP23-343I17 by recombination-mediated genetic engineering in *E. coli*; a 217-bp fragment containing the C-terminal tag sequences (fused in frame to the last *Bhlhe41* codon) and a 1.9-kb fragment containing the promoter of the mouse phosphoglycerate kinase (*Pgk1*) promoter linked to the neomycin-resistance gene (flanked by *lox*P sites). The tag sequences contained epitopes for Flag and V5 antibodies, two cleavage sites for the TEV protease and a biotin acceptor sequence (Biotin) for biotinylation by the *E. coli* biotin ligase BirA. In a second step, the targeting vector was generated by excision and insertion of the integrated sequences together with the flanking 5′ (4.7 kb) and 3′ (1.9 kb) homology regions by recombination-mediated genetic engineering from the modified BAC into the pBV-DTA-pA plasmid containing a gene encoding the herpes simplex virus thymidine kinase (for negative selection). DNA (15 μg) linearized with SgrA1 was transfected by electroporation into cells ($1 \times 10^7$) of the hybrid C57BL/6 x 129Sv ES cell line A9, followed by selection with 250 μg/ml G418. PCR-positive clones were verified by Southern blot analysis prior to injection into C57BL/6 blastocysts and the generation of $Bhlhe41^{Tag\text{-}neo/+}$ mice. The $Bhlhe41^{Tag}$ allele was obtained by crossing $Bhlhe41^{Tag\text{-}neo/+}$ mice with $Meox2^{Cre/+}$ mice53. The following primers were used for PCR genotyping of $Bhlhe41^{Tag/+}$ mice: 5′-CTCAGGAAGATGCCACGCAG-bp -3′ (a), 5′-ATTCCACATGGCTCTCCCAC-3′ (b). The $Bhlhe41^{Tag}$ allele was identified as a 665-bp PCR fragment and the wild-type *Bhlhe41* allele as a 384-bp PCR fragment by using the primer pair a/b.

## Antibodies

Monoclonal antibodies specific for B220/CD45R (RA3-6B2), CD2 (LFA-2), CD4 (GK1.5), CD5 (53-7.3), CD8α (53-6.7), CD11b (M1/70), CD11c (N418 and HL3), CD19 (6D5 and 1D3), CD21 (7G6), CD23 (B3B4), CD25 (PC61), CD28 (37.51), CD45.1 (A20), CD45.2 (104), CD72 (K10.6), CD93 (AA4.1), CD117/c-Kit (2B8), CD123/IL-3Rα (5B11), CD125/IL-5Rα (T21), CD138 (281-2), Gr-1 (RB6-8C5), IgD (11.26), IgM (II/41), NK1.1 (PK136), Sca-1 (D7), TCRβ (H57-597), TCRγδ (GL3), Ter119 (Ter119), human CD2 (RPA-2.10), Ki67 (SolA15), BLNK phosphorylated at Tyr84 (J117-1278), Erk1/2 phosphorylated at Thr202/Tyr204 (20A), phosphorylated PLCγ2 (K86-1161), Syk phosphorylated at Tyr525/526 (C87C1) and Btk phosphorylated at Tyr551 (M4G3LN) were purchased from BD Biosciences, eBioscience, Cell Signaling Technology or Biolegend.

Anti-$V_H12$ antibody (5C5; a kind gift of K. Rajewsky, Max-Delbrück Center for Molecular Medicine) was conjugated to Alexa-Fluor 647 with the Antibody Labeling Kit from Invitrogen. FITC-labeled phosphatidylcholine-containing liposomes were generated as described previously54. Texas Red-labeled phosphatidylcholine-containing liposomes were purchased from FormuMax.

## Definition of cell types by flow cytometry

Lymphocyte populations, unless stated otherwise, were gated as follows: CD4 T cells ($TCR\beta^+CD4^+$), CD8 T cells ($TCR\beta^+CD8\alpha^+$), NK cells ($TCR\beta^-TCR\gamma\delta^-NK1.1^+$), LSK cells ($CD4^-CD8^-TCR\beta^-TCR\gamma\delta^-NK1.1^-CD19^-CD11b^-CD11c^-Gr\text{-}1^-Ter119^-c\text{-}Kit^+Sca\text{-}1^+$), B-1-specified progenitors ($CD4^-CD8^-TCR\beta^-$ $CD11b^-Gr\text{-}1^-Ter119^-$

IgM$^{-}$CD19$^{+}$CD93$^{+}$B220$^{-/lo}$), pro-B cells (IgM$^{-}$IgD$^{-}$CD19$^{+}$B220$^{+}$c-Kit$^{+}$CD25$^{-}$ or IgM$^{-}$IgD$^{-}$CD19$^{+}$B220$^{+}$c-Kit$^{+}$CD2$^{-}$), pre-B cells (IgM$^{-}$IgD$^{-}$CD19$^{+}$B220$^{+}$c-Kit$^{-}$CD25$^{+}$ or IgM$^{-}$IgD$^{-}$CD19$^{+}$B220$^{+}$c-Kit$^{-}$CD2$^{+}$), bone marrow immature B cells (CD19$^{+}$IgD$^{-}$IgM$^{+}$), splenic T1 B cells (CD19$^{+}$B220$^{hi}$CD23$^{-}$CD21$^{-}$IgM$^{hi}$), splenic T2 B cells (CD19$^{+}$B220$^{hi}$CD23$^{+}$IgM$^{hi}$), splenic transitional B-1a cells (CD93$^{+}$IgM$^{+}$(CD19$^{+}$)B220$^{lo}$CD5$^{+}$), splenic FO B cells (CD19$^{+}$B220$^{hi}$CD23$^{+}$CD21$^{lo}$ or CD19$^{+}$B220$^{hi}$CD23$^{+}$CD21$^{lo}$IgD$^{hi}$IgM$^{lo}$), splenic MZ B cells (CD19$^{+}$B220$^{hi}$CD23$^{lo}$CD21$^{hi}$), splenic B-1a cells (CD19$^{+}$B220$^{lo}$), plasma cells (CD11c$^{-}$Gr1$^{-}$CD4$^{-}$CD8$^{-}$CD21$^{-}$CD138$^{+}$CD28$^{+}$), peritoneal B-2 cells (CD19$^{+}$B220$^{hi}$ or CD19$^{+}$CD23$^{+}$CD5$^{-}$), total peritoneal B-1 cells (CD19$^{+}$B220$^{lo}$), peritoneal B-1a cells (CD19$^{+}$B220$^{lo}$CD5$^{+}$ or CD19$^{+}$CD23$^{-}$CD5$^{+}$), peritoneal B-1b cells (CD19$^{+}$B220$^{lo}$CD5$^{-}$ or CD19$^{+}$CD23$^{-}$CD5$^{-}$).

Flow cytometric analysis was performed on FACS LSR Fortessa instruments (BD Biosciences), and sorting was performed on FACS Aria III (BD Biosciences) or Sony SH800 (Sony Biotechnology) cell sorters. Data were analyzed using FlowJo software (Treestar).

## Intracellular staining

Staining with 7-AAD and anti-Ki67 antibody (SolA15) was performed after fixation/permeabilization with the Foxp3 staining buffer set (eBioscience). Staining for phosphorylated BCR signaling components was performed on peritoneal cells isolated with ice-cold FACS buffer (2% FCS in PBS) and stained for CD19, B220 and CD5 on ice. The ice-cold cell suspension was mixed with an equal volume of pre-warmed Cytofix buffer (BD) and fixed for 15 minutes at 37 °C. Cells were washed with Perm/Wash Buffer I (BD) and stained in this buffer with antibodies against IgM and phosphorylated BCR signaling components for at least one hour at 23 °C.

## Generation of bone marrow and fetal liver chimeras

To generate mixed fetal liver chimeras, E14.5 fetal liver cells from wild-type B6.SJL (CD45.1) and *Bhlhe41*$^{-/-}$ *Bhlhe40*$^{-/-}$ (CD45.2) mice were mixed at a 1:1 ratio and transferred intravenously into lethally irradiated (1,000 Rads) *Rag2*$^{-/-}$ recipients. To generate mixed bone marrow chimeras, bone marrow cells from mice with the aforementioned genotypes were stained with IgM, CD4, CD8α, TCRβ, TCRγδ, and NK1.1 PE-labeled antibodies followed by magnetic depletion with anti-PE MicroBeads (Miltenyi Biotec). Cells were mixed at a 1:1 ratio and transferred intravenously into lethally irradiated *Rag2*$^{-/-}$ recipients. To generate “10% chimeras”, $V_H$12/Vκ4 transgenic wild-type or DKO bone marrow cells (CD45.2) were stained with CD4, CD8α, TCRβ, TCRγδ, NK1.1, IgM and $V_H$12 antibodies and sorted by flow cytometry against cells expressing these markers. These cells were then mixed at a 1:9 ratio with T and NK cell-depleted bone marrow from wild-type B6.SJL (CD45.1) mice and injected intravenously into lethally irradiated B6.SJL recipients.

## Adoptive cell transfer experiments

Equal numbers ($10^5$ cells) of flow cytometry-sorted CD45.2 wild-type and DKO peritoneal CD19$^{+}$CD5$^{+}$CD23$^{-}$ B-1a cells were transferred into sublethally irradiated (300 Rads) wild-

type B6.SJL recipients (CD45.1). The frequency of donor B cells ($CD19^+CD45.1^-CD45.2^+$) within total peritoneal B cells was analyzed at one and two months after transfer.

### *In vitro* stimulation and survival experiments

For flow cytometric analysis of *Bhlhe41* reporter expression, $hCD2^-$ FO B cells from *Bhlhe41*-iCre-IRES-hCD2 and wild-type mice were sorted by flow cytometry, seeded at a density of $5 \times 10^5$ cells/ml in the presence of 25 μg/ml LPS or 10 μg/ml anti-IgM and 20 ng/ml IL-4 or 2 μg/ml anti-CD40 antibody (eBioscience, HM40-3) and 20 ng/ml IL-4 or left unstimulated. hCD2 expression was assessed by flow cytometric analysis at days 2 and 4 of *in vitro* stimulation. For *in vitro* survival experiments, $V_H12/V\kappa4$ transgenic wild-type and DKO $CD19^+$ cells were sorted by flow cytometry and cultured overnight in the presence or absence of IL-5 (10 ng/ml). Cell death was assessed by staining with 7-ADD followed by flow cytometric analysis. All experiments were performed in IMDM medium containing 10% fetal calf serum, 1 mM glutamine and 50 μM β-mercaptoethanol. *Ex vivo* cell death was assessed by using the Violet Ratiometric Membrane Asymmetry Probe/Dead Cell Apoptosis kit together the MitoProbe DiIC1(5) kit (both from ThermoFisher Scientific) according to the manufacturer's instructions. Peritoneal cells from 10% chimeras were pre-stained with antibodies against CD19 and CD45.2 to gate on the $V_H12/V\kappa4$ transgenic donor B cells.

### Calcium fluorimetry

Splenic $V_H12/V\kappa4$ transgenic wild-type and DKO B-1a cells were stained with antibodies against CD19, B220 and CD5, and $2 \times 10^6$ cells were loaded with the calcium sensor dye eFluor 514 (eBioscience) at a final concentration of 1 μM in 1 ml of medium. After incubation at 37 °C for 40 min, the cells were washed and the fluorescent emission at 530/30 nm (excitation at 488 nm) was measured in live cells on a Fortessa flow cytometer. The acquisition of the data was initiated 40 sec prior to the addition of a goat anti-mouse IgM $F(ab')_2$ fragment (Jackson ImmunoResearch Laboratories). The data were collected for 180 sec and analyzed using the FlowJo software.

### RNA-seq analysis

All RNA-seq experiments were performed with sorted peritoneal B-1a cells, as previously described35 with minor modifications. In brief, RNA was isolated with an RNeasy Plus Mini Kit (Qiagen), and mRNA was obtained by poly(A) selection with a Dynabeads mRNA purification kit (Invitrogen), followed by fragmentation by heating at 94 °C for 3 min (in fragmentation buffer). The fragmented mRNA was used as template for first-strand cDNA synthesis with random hexamers and a Superscript VILO cDNA Synthesis kit (Invitrogen). The second-strand cDNA was synthesized with 100 mM dATP, dCTP, dGTP and dUTP in the presence of RNase H, *E. coli* DNA polymerase I and DNA ligase (Invitrogen). Sequencing libraries were prepared with the NEBNext Quick Ligation Module, NEBNext Endrepair Module and NEBNext dA-tailing module or NEBNext Ultra Ligation Module and NEBNext End Repair/dA-tailing module. For strand-specific RNA-sequencing, the uridines present in one cDNA strand were digested with uracil-N-glycosylase (New England Biolabs) as described55 followed by PCR amplification with the KAPA Real Time Amplification kit (KAPA Biosystems). Completed libraries were quantified with the Agilent Bioanalyzer




Europe PMC Funders Author Manuscripts

dsDNA 1000 assay kit and Agilent QPCR NGS Library Quantification kit. Cluster generation and sequencing was carried out by using the Illumina HiSeq 2000 system with a read length of 50 nucleotides according to the manufacturer's guidelines.

For V segment usage analysis (Fig. 2a,b), cDNA libraries were prepared from peritoneal B-1a cells isolated from 4 individual wild-type and 4 individual DKO mice of the same age. For the RNA-seq analysis shown in Figs. 5-8 and Supplementary Figs. 3-8, peritoneal wild-type and DKO B-1a cells were pooled from multiple sex- and age-matched mice, and two pooled samples for each genotype were sequenced.

### ChIP-seq analysis of Bhlhe41 binding

Splenic B-1a cells from $V_H12/V\kappa4$ transgenic *Bhlhe41*$^{Tag/Tag}$ mice were enriched by magnetic depletion of cell of other lineages. To this end, splenocytes were stained with a cocktail of PE-labeled antibodies against CD23, CD4, CD8, TCRβ, TCRγδ, NK1.1, CD11c, CD11b, Gr-1 and Ter119 followed by magnetic depletion with anti-PE MicroBeads (Miltenyi Biotec). Chromatin from $6 \times 10^7$ B-1a cells was prepared using a lysis buffer containing 0.25% SDS. The cells were subjected to ChIP as described56 with minor modifications. Anti-V5 agarose beads (Sigma-Aldrich) were used for precipitation. Sequencing libraries were prepared with the NEBNext Ultra Ligation Module and NEBNext End Repair/dA-tailing module followed by PCR amplification with the KAPA Real Time Amplification kit (KAPA Biosystems) and Illumina deep sequencing.

### Mapping of open chromatin regions by ATAC-seq

Open chromatin regions were mapped in sorted $V_H12/V\kappa4$ transgenic wild-type and DKO B-1a cells from the spleen of bone marrow chimeras by ATAC-seq, as described39 with the following modification. The nuclei were prepared by incubation of cells with nuclear preparation buffer (0.30 M sucrose, 10 mM Tris, pH 7.5, 60 mM KCl, 15 mM NaCl, 5 mM $MgCl_2$, 0.1 mM EGTA, 0.1% NP40, 0.15 mM spermine, 0.5 mM spermidine and 2 mM 6AA) before the Tn5 treatment ($3 \times 10^4$ cells with 4 μl of the Nextera Tn5 transposase).

### Gene set enrichment analysis

Gene Set Enrichment Analysis was performed using the GSEA software from the Broad Institute57. Genes were ranked based on their $\log_2$ fold change from the DESeq2 package and either compared to sets from the MSigDB or our own defined gene sets.

### Analysis of ChIP-seq data

For ChIP-seq, the reads were aligned to the mouse genome assembly version of July 2007 (NCBI37/mm9), using the Bowtie program version 12.5. Peaks were called with a *P* value of $< 10^{-10}$ by using the MACS program version 1.3.6.1 (ref. 58) with default parameters, a genome size of 2,654,911,517 bp (mm9) and a pro-B cell input sample. The identified peaks were then assigned to target genes as described59. Bhlhe41 peaks overlapping with the transcription start site (TS) were referred to as promoter peaks in Fig. 5b.

### Analysis of ATAC-seq data

For alignment of ATAC-seq reads, the Bowtie version 2.1.0 was used with the additional parameter −sensitive −X 5000. Insert sizes were extracted from the aligned BAM files with SAMtools version 0.1.18 (ref. 60) and analyzed with R version 3.1.1 (http://www.R-project.org.) to determine the fragment sizes associated with nucleosome free positions. After removing fragments above 1 kb, a random subsample of 50,000 values was drawn from each alignment. The h.crit function from the silvermantest package (version 1.0) was used to determine the bandwidth for k=6 modes in the density function of the fragment size distribution. These modes were used as means for fitting k=6 normal distributions to the observed fragment sizes using the normalmixEM function from the mixtools package version 1.0.2. With these parameters, the fragment size boundaries were fixed so that no more than 80% of each partition overlapped with its neighbors analogous to the analysis previously described39. Only the first read of read pairs with an estimated fragment size below 150 have been used for calling peaks using MACS as described above. Peaks were overlapped using the Multovl program61.

### Motif analysis

For motif discovery, we used the MEME-ChIP suite (version 4.9.1)62 to predict the most significant motifs present in the 300 bp centered at the peak summit of the top 300 sequences, as sorted by the fold enrichment score of the MACS program.

### Bioinformatic analysis of RNA-seq data

Sequence reads that passed the Illumina quality filtering were considered for alignment. Reads corresponding to mouse ribosomal RNAs (BK000964.1 and NR046144.1) were removed. The remaining reads were cut down to a read length of 44 bp and aligned to the mouse transcriptome (genome assembly version of July 2007 NCBI37/mm9) using TopHat version 1.4.1 (ref. 63).

The calculation of RNA expression values was all based on the RefSeq database, which was downloaded from UCSC on January 10th, 2014. The annotation of immunoglobulin and T cell receptor genes was incorporated from the Ensembl release 67 (ref. 64). Genes with overlapping exons were flagged and double entries (i.e. exactly the same gene at two different genomic locations) were renamed. Genes with several transcripts were merged to consensus-genes consisting of a union of all underlying exons using the fuge software (I. Tamir, unpublished), which resulted in 25,726 gene models.

For analysis of differential gene expression, the number of reads per gene was counted using HTseq version 0.5.3 (ref. 65) with the overlap resolution mode set to ‘union’. The datasets were analyzed using the R package DESeq2 version 1.4.1 (ref. 66). Sample normalizations and dispersion estimations were conducted using the default DESeq2 settings. Transcripts per million (TPM) were calculated from RNA-seq data, as described67, in order to compare the expression of *Bhlhe40* and *Bhlhe41* among the different hematopoietic cell types shown in Supplementary Fig. 1c.

For principal component analysis (PCA), gene counts were transformed into regularized log values with the R package DESeq2 version 1.8.2 (ref. 66). The 500 most varying genes for wild-type B cell subsets (FO B, MZ B, and B-1a cells) were then considered for PCA. Immunoglobulin and T cell receptor genes were excluded from the analysis. Very similar results were obtained when DKO and/or $V_H12/V\kappa4$ transgenic B-1a cells were used together with the wild-type B cell subsets (Supplementary Figs. 3a and 4b).

### Statistical analysis

Statistical analysis was performed with the GraphPad Prism 7 software. Statistical significance of differences between two experimental groups in all experiments, with the exception of those involving NGS-based approaches, was assessed by two-tailed Student's *t*-test analysis. The statistical evaluation of the RNA-seq data is described in the section dealing with the bioinformatic analysis of RNA-seq data.

### Data availability

RNA-seq, ChIP-seq and ATAC-seq data first reported in this study are available at the Gene Expression Omnibus (GEO) repository under the accession numbers GSE93764. Previously published datasets, which were used in this study, are available at the GEO repository under the accession numbers GSE77744 and GSE35857. Source data for Figures 1–4, 6, 7, 8 are provided with the paper.

## Supplemental Information

Refer to Web version on PubMed Central for supplementary material.

## Acknowledgements

We thank S.H. Clarke and S.-R. Lee (University of North Carolina at Chapel Hill, USA) and H. Wang (National Institute of Allergy and Infectious Diseases, National Institutes of Health, USA) for providing the $V_H12$ and $V\kappa4$ transgenic mice, K. Rajewsky for the anti-$V_H12$ antibody, K. Schindler for help with signaling experiments, M. Fischer for bioinformatic analysis, C. Theussl for the generation of transgenic mice, K. Aumayr and her colleagues for flow cytometric sorting and A. Sommer and his colleagues (Vienna Biocenter Core Facilities GmbH) for Illumina sequencing. This research was supported by Boehringer Ingelheim, an ERC Advanced Grant (291740-LymphoControl; to M.B.) from the European Community's Seventh Framework Program, the Austrian Industrial Research Promotion Agency (Headquarter Grant FFG-852936; to M.B.), the Austrian Science Fund (P28841; to T.K.), and a Marie-Curie fellowship (PIIF-GA-2013-628065; to T.K).

## References

1. Hayakawa K, Hardy RR, Parks DR, Herzenberg LA. The "Ly-1 B" cell subpopulation in normal immunodefective, and autoimmune mice. J Exp Med. 1983; 157:202–218. [PubMed: 6600267]
2. Baumgarth N. The double life of a B-1 cell: self-reactivity selects for protective effector functions. Nat Rev Immunol. 2011; 11:34–46. [PubMed: 21151033]
3. Montecino-Rodriguez E, Dorshkind K. B-1 B cell development in the fetus and adult. Immunity. 2012; 36:13–21. [PubMed: 22284417]
4. Casola S, et al. B cell receptor signal strength determines B cell fate. Nat Immunol. 2004; 5:317–327. [PubMed: 14758357]
5. Hardy RR, Hayakawa K. B cell development pathways. Annu Rev Immunol. 2001; 19:595–621. [PubMed: 11244048]
6. Hoffmann A, et al. Siglec-G is a B1 cell-inhibitory receptor that controls expansion and calcium signaling of the B1 cell population. Nat Immunol. 2007; 8:695–704. [PubMed: 17572677]

7. Pan C, Baumgarth N, Parnes JR. CD72-deficient mice reveal nonredundant roles of CD72 in B cell development and activation. Immunity. 1999; 11:495–50. [PubMed: 10549631]
8. Binder CJ. Natural IgM antibodies against oxidation-specific epitopes. J Clin Immunol. 2010; 30:56–60.
9. Wang H, Clarke SH. Positive selection focuses the $V_H12$ B-cell repertoire towards a single B1 specificity with survival function. Immunol Rev. 2004; 197:51–59. [PubMed: 14962186]
10. Sohlenkamp C, López-Lara IM, Geiger O. Biosynthesis of phosphatidylcholine in bacteria. Prog Lipid Res. 2003; 42:115–162. [PubMed: 12547654]
11. Lalor PA, Herzenberg LA, Adams S, Stall AM. Feedback regulation of murine Ly-1 B cell development. Eur J Immunol. 1989; 19:507–513. [PubMed: 2785046]
12. Kristiansen TA, et al. Cellular barcoding links B-1a B cell potential to a fetal hematopoietic stem cell state at the single-cell level. Immunity. 2016; 45:346–357. [PubMed: 27533015]
13. Yang Y, et al. Distinct mechanisms define murine B cell lineage immunoglobulin heavy chain (IgH) repertoires. eLife. 2015; 4:e09083. [PubMed: 26422511]
14. Gu H, Förster I, Rajewsky K. Sequence homologies, N sequence insertion and $J_H$ gene utilization in $V_HDJ_H$ joining: implications for the joining mechanism and the ontogenetic timing of Ly1 B cell and B-CLL progenitor generation. EMBO J. 1990; 9:2133–2140. [PubMed: 2113468]
15. Düber S, et al. Induction of B-cell development in adult mice reveals the ability of bone marrow to produce B-1a cells. Blood. 2009; 114:4960–4967. [PubMed: 19812384]
16. Herzenberg LA, Herzenberg LA. Toward a layered immune system. Cell. 1989; 59:953–954. [PubMed: 2688900]
17. Montecino-Rodriguez E, Leathers H, Dorshkind K. Identification of a B-1 B cell-specified progenitor. Nat Immunol. 2006; 7:293–301. [PubMed: 16429139]
18. Montecino-Rodriguez E, et al. Distinct genetic networks orchestrate the emergence of specific waves of fetal and adult B-1 and B-2 development. Immunity. 2016; 45:527–539. [PubMed: 27566938]
19. Haughton G, Arnold LW, Whitmore AC, Clarke SH. B-1 cells are made, not born. Immunol Today. 1993; 14:84–87. [PubMed: 7680563]
20. Hayakawa K, et al. Positive selection of natural autoreactive B cells. Science. 1999; 285:113–116. [PubMed: 10390361]
21. Berland R, Wortis HH. Origins and functions of B-1 cells with notes on the role of CD5. Annu Rev Immunol. 2002; 20:253–300. [PubMed: 11861604]
22. Zhou Y, et al. Lin28b promotes fetal B lymphopoiesis through the transcription factor Arid3a. J Exp Med. 2015; 212:569–580. [PubMed: 25753579]
23. Yuan J, Nguyen CK, Liu X, Kanellopoulou C, Muljo SA. Lin28b reprograms adult bone marrow hematopoietic progenitors to mediate fetal-like lymphopoiesis. Science. 2012; 335:1195–1200. [PubMed: 22345399]
24. Humbert PO, Corcoran LM. *oct-2* gene disruption eliminates the peritoneal B-1 lymphocyte lineage and attenuates B-2 cell maturation and function. J Immunol. 1997; 159:5273–5284. [PubMed: 9548466]
25. Pedersen GK, et al. B-1a transitional cells are phenotypically distinct and are lacking in mice deficient in IκBNS. Proc Natl Acad Sci USA. 2014; 111:E4119–E4126. [PubMed: 25228759]
26. Kato Y, Kawamoto T, Fujimoto K, Noshiro M. DEC1/STRA13/SHARP2 and DEC2/SHARP1 coordinate physiological processes, including circadian rhythms in response to environmental stimuli. Curr Top Dev Biol. 2014; 110:339–372. [PubMed: 25248482]
27. Ow JR, Tan YH, Jin Y, Bahirvani AG, Taneja R. Stra13 and Sharp-1, the non-grouchy regulators of development and disease. Curr Top Dev Biol. 2014; 110:317–338. [PubMed: 25248481]
28. Sun H, Lu B, Li RQ, Flavell RA, Taneja R. Defective T cell activation and autoimmune disorder in Stra13-deficient mice. Nat Immunol. 2001; 2:1040–1047. [PubMed: 11668339]
29. Yang XO, et al. Requirement for the basic helix-loop-helix transcription factor Dec2 in initial $T_H2$ lineage commitment. Nat Immunol. 2009; 10:1260–1266. [PubMed: 19881507]
30. Lin C-C, et al. Bhlhe40 controls cytokine production by T cells and is essential for pathogenicity in autoimmune neuroinflammation. Nat Commun. 2014; 5:3551. [PubMed: 24699451]

31. Vilagos B, et al. Essential role of EBF1 in the generation and function of distinct mature B cell types. J Exp Med. 2012; 209:775–792. [PubMed: 22473956]
32. Heng TS, Painter MW, Immunological Genome Project Consortium. The Immunological Genome Project: networks of gene expression in immune cells. Nat Immunol. 2008; 9:1091–1094. [PubMed: 18800157]
33. Baier PC, et al. Mice lacking the circadian modulators SHARP1 and SHARP2 display altered sleep and mixed state endophenotypes of psychiatric disorders. PLoS One. 2014; 9:e110310. [PubMed: 25340473]
34. Honma S, et al. Dec1 and Dec2 are regulators of the mammalian molecular clock. Nature. 2002; 419:841–844. [PubMed: 12397359]
35. Wöhner M, et al. Molecular functions of the transcription factors E2A and E2-2 in controlling germinal center B cell and plasma cell development. J Exp Med. 2016; 213:1201–1221. [PubMed: 27261530]
36. Seimiya M, et al. Clast5/Stra13 is a negative regulator of B lymphocyte activation. Biochem Biophys Res Commun. 2002; 292:121–127. [PubMed: 11890681]
37. Arnold LW, Pennell CA, McCray SK, Clarke SH. Development of B-1 cells: segregation of phosphatidylcholine-specific B cells to the B-1 population occurs after immunoglobulin gene expression. J Exp Med. 1994; 179:1585–1595. [PubMed: 8163938]
38. Jolma A, et al. DNA-binding specificities of human transcription factors. Cell. 2013; 152:327–339. [PubMed: 23332764]
39. Buenrostro JD, Giresi PG, Zaba LC, Chang HY, Greenleaf WJ. Transposition of native chromatin for fast and sensitive epigenomic profiling of open chromatin, DNA-binding proteins and nucleosome position. Nat Methods. 2013; 10:1213–1218. [PubMed: 24097267]
40. Holodick NE, Tumang JR, Rothstein TL. Continual signaling is responsible for constitutive ERK phosphorylation in B-1a cells. Mol Immunol. 2009; 46:3029–3036. [PubMed: 19592097]
41. Wong S-C, et al. Peritoneal $CD5^+$ B-1 cells have signaling properties similar to tolerant B cells. J Biol Chem. 2002; 277:30707–30715. [PubMed: 12070149]
42. Chew V, Lam K-P. Leupaxin negatively regulates B cell receptor signaling. J Biol Chem. 2007; 282:27181–27191. [PubMed: 17640867]
43. Rickert RC, Rajewsky K, Roes J. Impairment of T-cell-dependent B-cell responses and B-1 cell development in CD19-deficient mice. Nature. 1995; 376:352–355. [PubMed: 7543183]
44. Yoshida T, et al. Defective B-1 cell development and impaired immunity against Angiostrongylus cantonensis in IL-5Rα-deficient mice. Immunity. 1996; 4:483–494. [PubMed: 8630733]
45. Moon, B-g, Takaki, S., Miyake, K., Takatsu, K. The role of IL-5 for mature B-1 cells in homeostatic proliferation, cell survival, and Ig production. J Immunol. 2004; 172:6020–6029. [PubMed: 15128785]
46. Scott CL, et al. Reassessment of interactions between hematopoietic receptors using common beta-chain and interleukin-3-specific receptor beta-chain-null cells: no evidence of functional interactions with receptors for erythropoietin, granulocyte colony-stimulating factor, or stem cell factor. Blood. 2000; 96:1588–1590. [PubMed: 10942411]
47. Arnold LW, McCray SK, Tatu C, Clarke SH. Identification of a precursor to phosphatidyl choline-specific B-1 cells suggesting that B-1 cells differentiate from splenic conventional B cells in vivo: cyclosporin A blocks differentiation to B-1. J Immunol. 2000; 164:2924–2930. [PubMed: 10706678]
48. Guo B, Rothstein TL. RasGRP1 Is an essential signaling molecule for development of B1a cells with autoantigen receptors. J Immunol. 2016; 196:2583–2590. [PubMed: 26851222]
49. Seimiya M, et al. Impaired lymphocyte development and function in Clast5/Stra13/DEC1-transgenic mice. Eur J Immunol. 2004; 34:1322–1332. [PubMed: 15114665]
50. Hipfner DR, Cohen SM. Connecting proliferation and apoptosis in development and disease. Nat Rev Mol Cell Biol. 2004; 5:805–815. [PubMed: 15459661]
51. Rossner MJ, et al. Disturbed clockwork resetting in Sharp-1 and Sharp-2 single and double mutant mice. PLoS One. 2008; 3:e2762. [PubMed: 18648504]
52. Kwon K, et al. Instructive role of the transcription factor E2A in early B lymphopoiesis and germinal center B cell development. Immunity. 2008; 28:751–762. [PubMed: 18538592]

53. Tallquist MD, Soriano P. Epiblast-restricted Cre expression in MORE mice: a tool to distinguish embryonic vs. extra-embryonic gene function. Genesis. 2000; 26:113–115. [PubMed: 10686601]
54. Kretschmer K, Stopkowicz J, Scheffer S, Greten TF, Weiss S. Maintenance of peritoneal B-1a lymphocytes in the absence of the spleen. J Immunol. 2004; 173:197–204. [PubMed: 15210775]
55. Parkhomchuk D, et al. Transcriptome analysis by strand-specific sequencing of complementary DNA. Nucleic Acids Res. 2009; 37:e123. [PubMed: 19620212]
56. Schebesta A, et al. Transcription factor Pax5 activates the chromatin of key genes involved in B cell signaling, adhesion, migration, and immune function. Immunity. 2007; 27:49–63. [PubMed: 17658281]
57. Subramanian A, et al. Gene set enrichment analysis: a knowledge-based approach for interpreting genome-wide expression profiles. Proc Natl Acad Sci USA. 2005; 102:15545–15550. [PubMed: 16199517]
58. Feng J, Liu T, Qin B, Zhang Y, Liu XS. Identifying ChIP-seq enrichment using MACS. Nat Protoc. 2012; 7:1728–1740. [PubMed: 22936215]
59. Revilla-i-Domingo R, et al. The B-cell identity factor Pax5 regulates distinct transcriptional programmes in early and late B lymphopoiesis. EMBO J. 2012; 31:3130–3146. [PubMed: 22669466]
60. Li H, et al. The sequence alignment/map format and SAMtools. Bioinformatics. 2009; 25:2078–2079. [PubMed: 19505943]
61. Aszodi A. MULTOVL: fast multiple overlaps of genomic regions. Bioinformatics. 2012; 28:3318–3319. [PubMed: 23071271]
62. Machanick P, Bailey TL. MEME-ChIP: motif analysis of large DNA datasets. Bioinformatics. 2011; 27:1696–1697. [PubMed: 21486936]
63. Trapnell C, Pachter L, Salzberg SL. TopHat: discovering splice junctions with RNA-Seq. Bioinformatics. 2009; 25:1105–1111. [PubMed: 19289445]
64. Cunningham F, et al. Ensembl 2015. Nucleic Acids Res. 2015; 43:D662–D669. [PubMed: 25352552]
65. Anders S, Pyl PT, Huber W. HTSeq--a Python framework to work with high-throughput sequencing data. Bioinformatics. 2015; 31:166–169. [PubMed: 25260700]
66. Love MI, Huber W, Anders S. Moderated estimation of fold change and dispersion for RNA-seq data with DESeq2. Genome Biol. 2014; 15:550. [PubMed: 25516281]
67. Wagner GP, Kin K, Lynch VJ. Measurement of mRNA abundance using RNA-seq data: RPKM measure is inconsistent among samples. Theory Biosci. 2012; 131:281–285. [PubMed: 22872506]

Europe PMC Funders Author Manuscripts

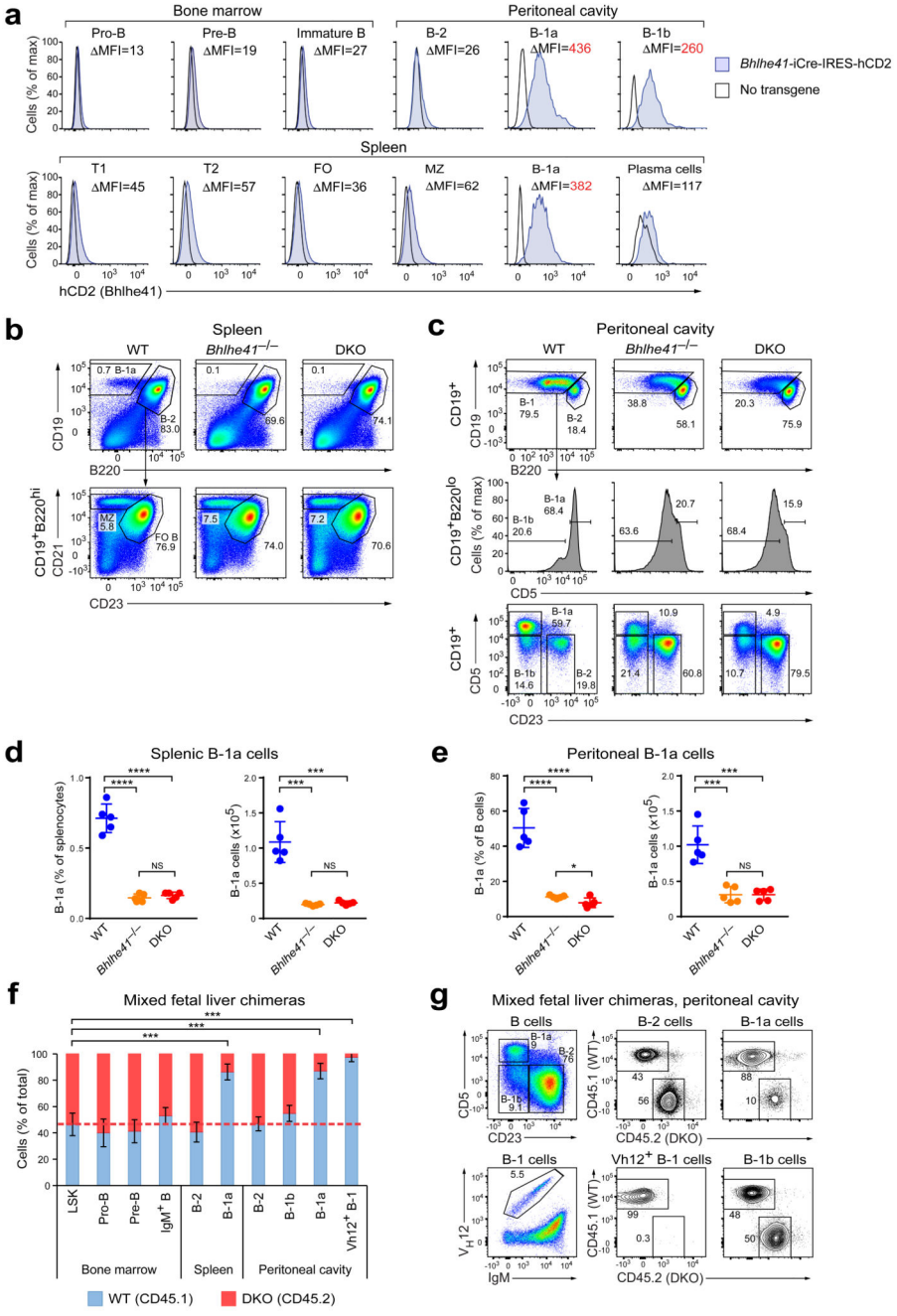


**Figure 1. B-1a cells depend on the transcription factors Bhlhe41 and Bhlhe40.**

(**a**) Cells from *Bhlhe41*-iCre-IRES-hCD2 transgenic and wild-type mice were stained with antibodies against human CD2 and markers defining the indicated cell populations. The flow cytometric definition of all cell types is described in the Online Methods. Histograms comparing hCD2 expression of the indicated cell types are shown. The difference in the median fluorescence intensity (ΔMFI) between *Bhlhe41*-iCre-IRES-hCD2 transgenic and wild-type cells of the indicated cell populations is shown for the pair of wild-type and reporter mice displayed in the plot. One representative result of two independent

experiments is shown, and six *Bhlhe41*-iCre-IRES-hCD2 transgenic mice were analyzed in total. (**b**-**e**) Distribution of B cell subsets among splenocytes (**b**,**d**) and peritoneal cells (**c**,**e**) from wild-type (WT), *Bhlhe41*$^{-/-}$ and *Bhlhe41*$^{-/-}$*Bhlhe40*$^{-/-}$ (DKO) mice. Gating is applied as indicated. (**b**,**d**) The distribution of B-1a, MZ and FO B cells among splenocytes (**b**), and the quantification of splenic B-1a cells (**d**) are shown. (**c**) The distribution of B-1a, B-1b and B-2 cells in the peritoneal cavity was analyzed with two alternative gating strategies. Numbers refer to the percentage of cells in the indicated gates. (**e**) Quantification of peritoneal B-1a cells, which were defined as CD19$^{+}$CD5$^{+}$CD23$^{-}$ cells as shown in the bottom row of (**c**). Horizontal bars indicate mean value, error bars represent SD. NS $P > 0.05$, * $P < 0.05$, *** $P < 0.001$, **** $P < 0.0001$, as determined by the Student's *t*-test. Five age-matched mice were analyzed per genotype. One representative result of five (**c**,**e**) and four (**b**,**d**) independent experiments is shown. (**f**,**g**) E14.5 fetal liver cells from DKO (CD45.2) and WT (CD45.1) embryos were mixed at a 1:1 ratio and injected into lethally irradiated *Rag2*$^{-/-}$ recipients. CD45.1 and CD45.2 expression was analyzed for the indicated cell populations 6 weeks after transfer. (**f**) Frequency of CD45.1$^{+}$ (WT) and CD45.2$^{+}$ (DKO) cells in the indicated bone marrow, splenic and peritoneal cell populations. Error bars represent SD, n = 6-7; *** $P < 0.001$ (Student's *t*-test). One representative result of two independent experiments is shown. (**g**) Representative FACS plots showing the gating of the indicated peritoneal B cell subsets and the frequencies of CD45.1$^{+}$ and CD45.2$^{+}$ cells within these populations.

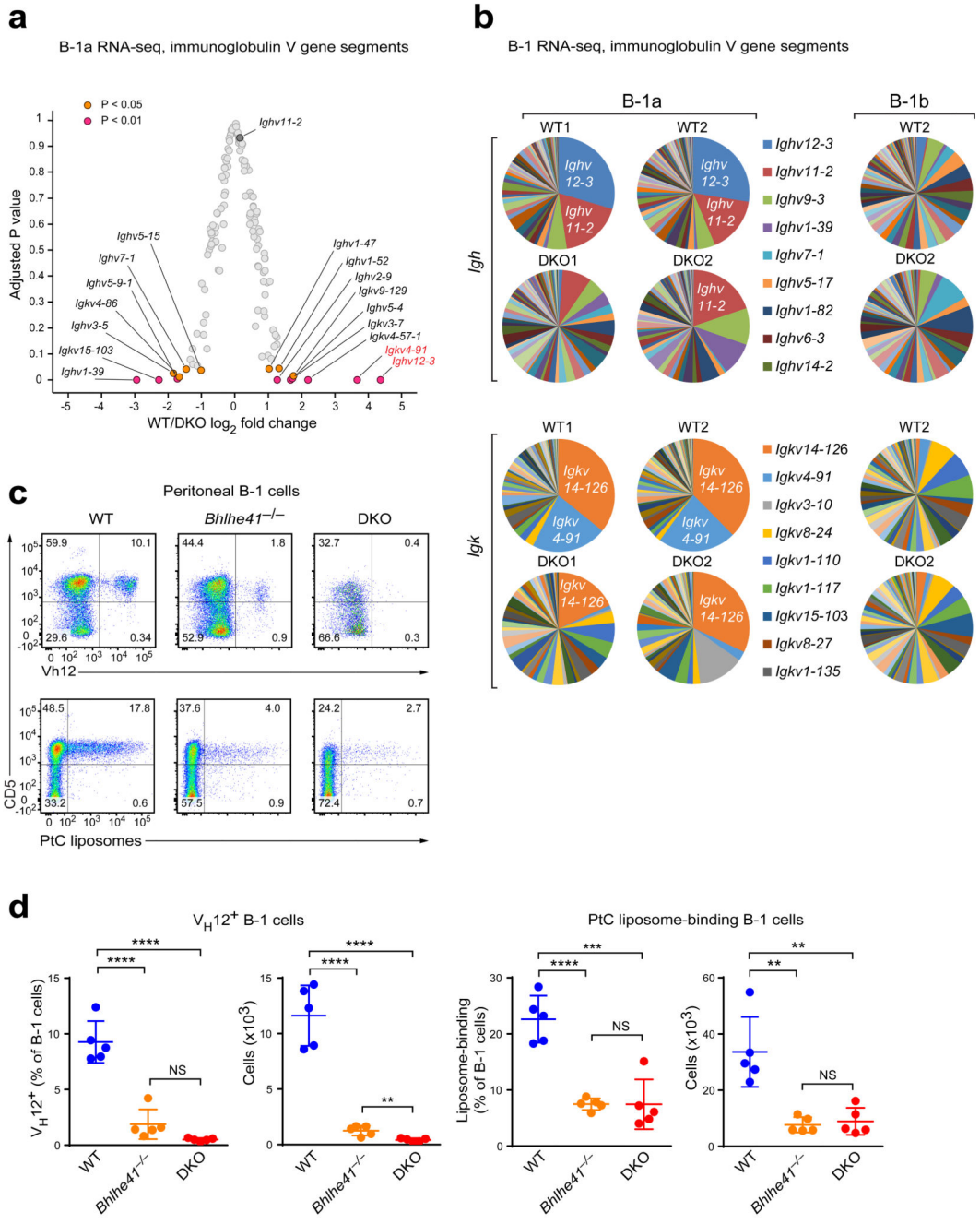


**Figure 2. The residual DKO B-1a cells exhibit an altered BCR repertoire.**

(**a**,**b**) Peritoneal B-1a cells were sorted from four wild-type and four DKO mice, and the sorted cells of each mouse were individually analyzed by RNA-seq. (**a**) Volcano plot showing expression changes ($log_2$-transformed values; horizontal axis) between wild-type (WT) and DKO cells and adjusted *P* values (vertical axis) for V gene segments of the immunoglobulin heavy-chain (*Igh*) and κ light-chain (*Igk*) loci. (**b**) Pie charts showing the distribution of RNA-seq reads in V segments of the *Igh* and *Igk* genes for B-1a cells from two pairs of wild-type and DKO mice (left) and for B-1b cells from one wild-type and DKO




Europe PMC Funders Author Manuscripts

mouse (right). The V genes are named according to the IMGT nomenclature. (**c**) Peritoneal cells from wild-type, *Bhlhe41*$^{-/-}$ and DKO mice were stained with antibodies against CD19, B220, CD5, IgM, and $V_H12$ or with FITC-loaded PtC-containing liposomes. Expression of CD5 and the $V_H12$ BCR, as well as binding of liposomes is shown for CD19$^{+}$B220$^{lo}$ B-1 cells. (**d**) Frequencies and absolute numbers of $V_H12^{+}$ B-1 cells (left) and liposome-binding B-1 cells (right). Horizontal bars indicate mean value, error bars represent SD. NS $P > 0.05$, ** $P < 0.01$, *** $P < 0.001$, **** $P < 0.0001$, as determined by the Student's *t*-test. Five age-matched mice were used per genotype. One representative result of four ($V_H12$ staining) and two (liposome staining) independent experiments is shown.

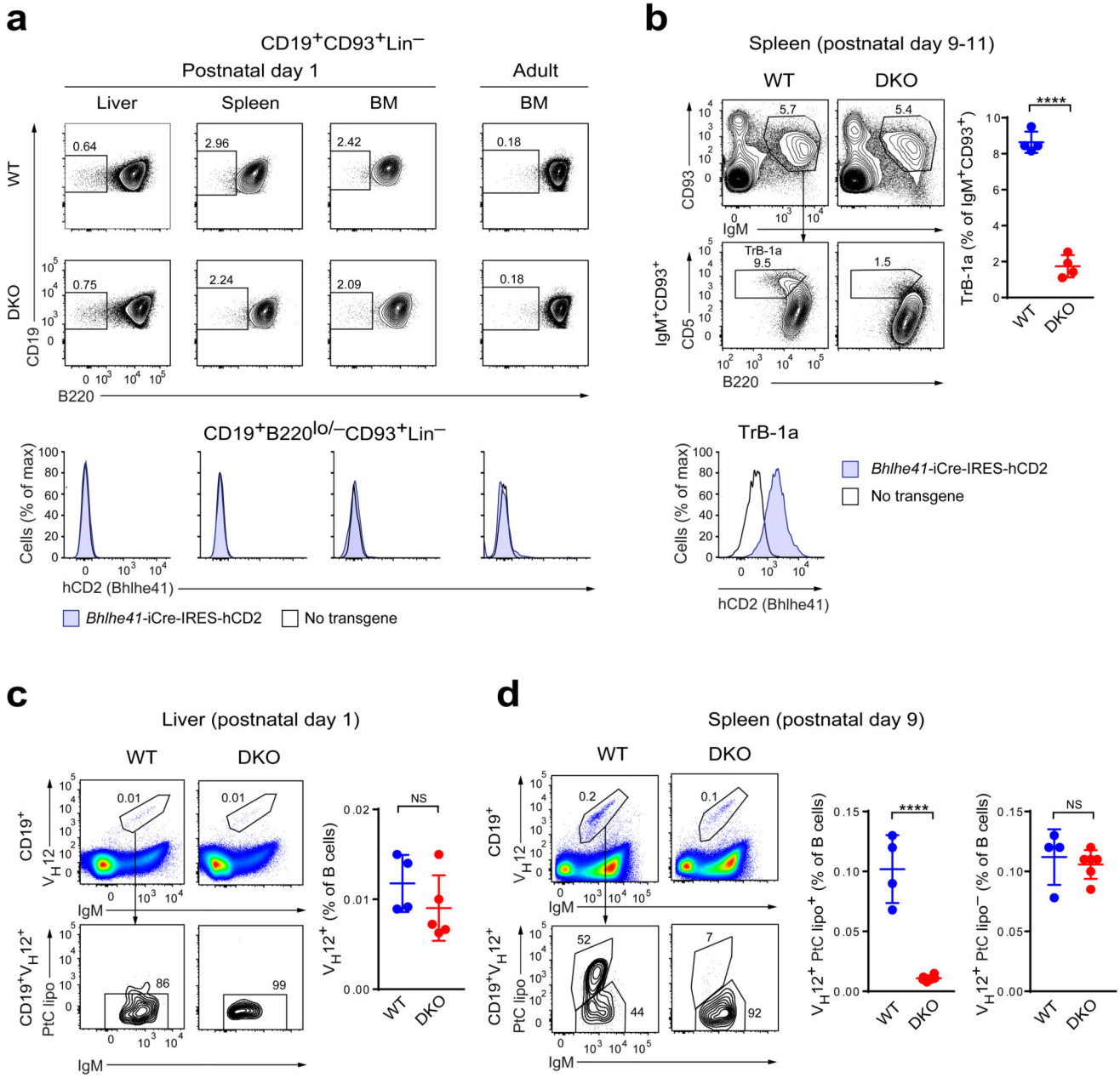


**Figure 3. Regulation of B-1a cell development by Bhlhe41 and Bhlhe40.**

(**a**) Flow cytometric analysis of Lin$^{-}$IgM$^{-}$CD93$^{+}$CD19$^{+}$B220$^{lo/-}$ B-1-specified progenitors17 in neonatal liver, spleen and bone marrow (BM) cells (postnatal day 1) as well as adult BM cells from wild-type (WT) and DKO mice (top and middle rows) or wild-type and *Bhlhe41*-iCre-IRES-hCD2 transgenic mice (bottom row). For gating strategy see Supplementary Fig. 3b. The frequency of B220$^{lo/-}$ cells among Lin$^{-}$IgM$^{-}$CD93$^{+}$CD19$^{+}$ B cells (top and middle rows) and the expression of hCD2 by Lin$^{-}$IgM$^{-}$CD93$^{+}$CD19$^{+}$B220$^{lo/-}$ cells are shown. One representative result of two independent experiments is shown. (**b**) Flow cytometric analysis of CD93$^{+}$IgM$^{+}$CD19$^{+}$B220$^{lo}$CD5$^{+}$ transitional B-1a cells (TrB-1a) in the neonatal spleen (postnatal day 9-11) from wild-type and DKO mice (top and middle

rows) or wild-type and *Bhlhe41*-iCre-IRES-hCD2 transgenic mice (bottom row). A representative plots (left) and the frequency of transitional B-1a cells among $CD93^+IgM^+$ splenocytes (right) are shown. Horizontal bars indicate mean value, error bars represent SD. **** $P < 0.0001$, as determined by the Student's *t*-test. Four mice were analyzed per genotype. The expression of hCD2 on transitional B-1a cells from *Bhlhe41*-iCre-IRES-hCD2 transgenic mice is shown for one representative result of two independent experiments. (**c**) Day-1 neonatal liver cells from wild-type and DKO mice were stained with antibodies against CD19, IgM, $V_H12$ and with PtC-containing liposomes (lipo). The frequency of $IgM^+V_H12^+$ cells among $CD19^+$ B cells (top and right) and the liposome binding by $CD19^+IgM^+V_H12^+$ cells (bottom) are shown. Horizontal bars indicate mean value, error bars represent SD. NS $P > 0.05$, as determined by the Student's *t*-test. One experiment was performed with 4 wild-type and 5 DKO mice. (**d**) Flow cytometric analysis of wild-type and DKO splenocytes at postnatal day 9, as described in (**c**). The frequencies of liposome-binding and non-binding $CD19^+IgM^+V_H12^+$ cells among $CD19^+$ B cells are shown to the right. Horizontal bars indicate mean value, error bars represent SD. NS $P > 0.05$, **** $P < 0.0001$, as determined by the Student's *t*-test. One representative analysis of 4 wild-type and 6 DKO mice of two independent experiments is shown.

Europe PMC Funders Author Manuscripts

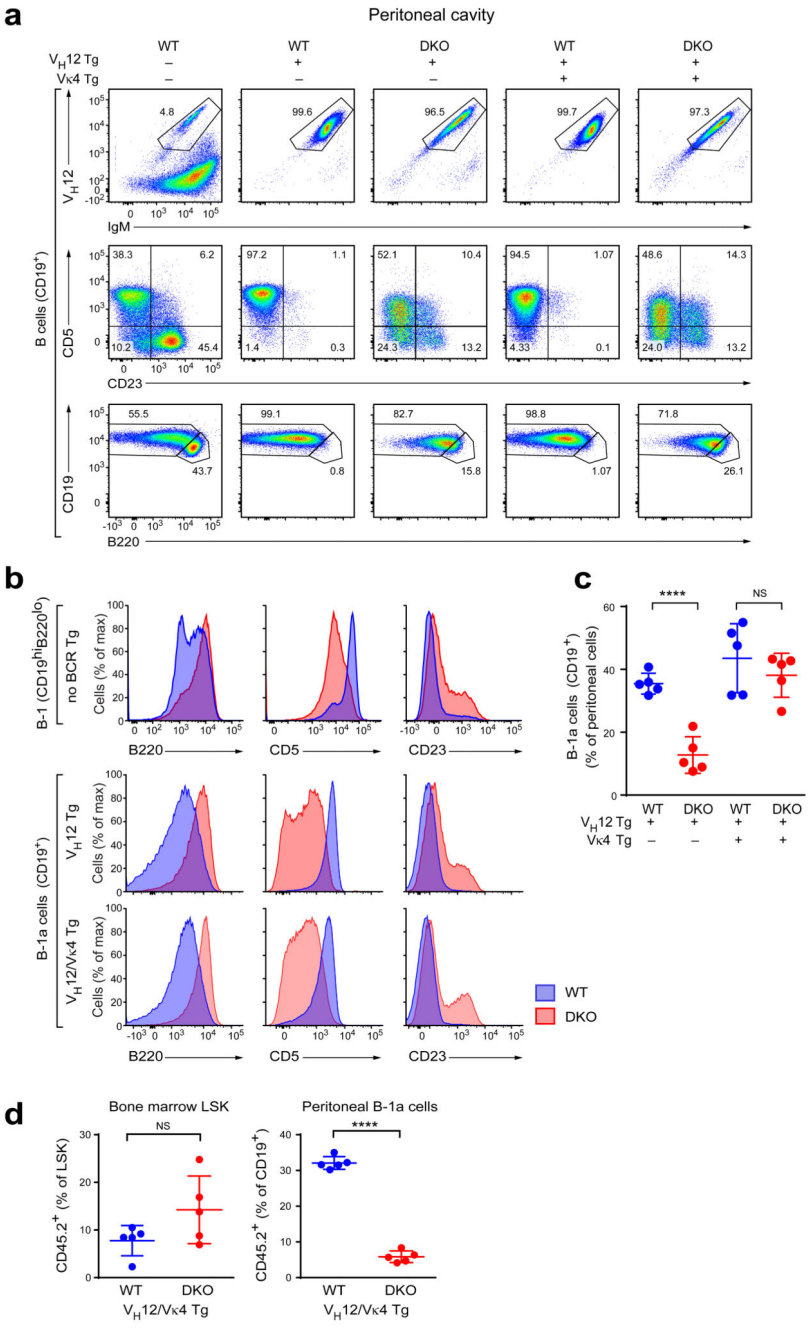


**Figure 4. Expression of pre-rearranged $V_H12$ and Vκ4 transgenes fails to rescue the DKO phenotype.**

(**a**) Peritoneal cells from mice of the indicated genotypes were stained with antibodies against $V_H12$, IgM, CD5, CD23, CD19, and B220 and were analyzed by flow cytometry. All plots are gated on $CD19^+$ cells. One representative result of four independent experiments is shown. (**b**) Histograms showing CD5, B220 and CD23 expression by non-transgenic peritoneal $CD19^{hi}B220^{lo}$ B-1a cells (top) and $V_H12$- and $V_H12/V\kappa4$-transgenic (middle and bottom) peritoneal B cells from wild-type (blue) and DKO (red) mice. Note that the non-

transgenic and BCR-transgenic cells were analyzed in different experiments, and hence a direct comparison of the absolute values of marker expression is not possible. A representative result of four ($V_H12$-transgenic and $V_H12/V\kappa4$-transgenic) and at least seven (polyclonal B-1a cells) independent experiments are shown. (**c**) Frequency of $CD19^+$ B cells among all peritoneal cells in mice of the indicated genotypes. Horizontal bars indicate mean value, error bars represent SD. NS $P > 0.05$; **** $P < 0.0001$, Student's *t*-test. Data are shown for five mice per genotype, which were analyzed in 4 independent experiments. (**d**) Lethally irradiated wild-type B6SJL mice (CD45.1) were injected with a 1:9 mixture of $V_H12/V\kappa4$ transgenic wild-type or DKO bone marrow cells (CD45.2) and non-transgenic wild-type bone marrow cells (CD45.1) depleted of T and NK cells. $V_H12/V\kappa4$ transgenic bone marrow cells were additionally depleted of $V_H12^+$ cells by flow cytometry sorting. The resulting "10% chimeras" were analyzed 6-8 weeks after bone marrow transfer. Frequencies of $CD45.2^+$ cells among bone marrow $Lin^-Sca1^+Kit^+$ (LSK) cells and peritoneal B cells are shown. Horizontal bars indicate mean value, error bars represent SD. NS $P > 0.05$; **** $P < 0.0001$, Student's *t*-test. Values for five mice per genotype are plotted. A representative result of two independent experiments is shown.

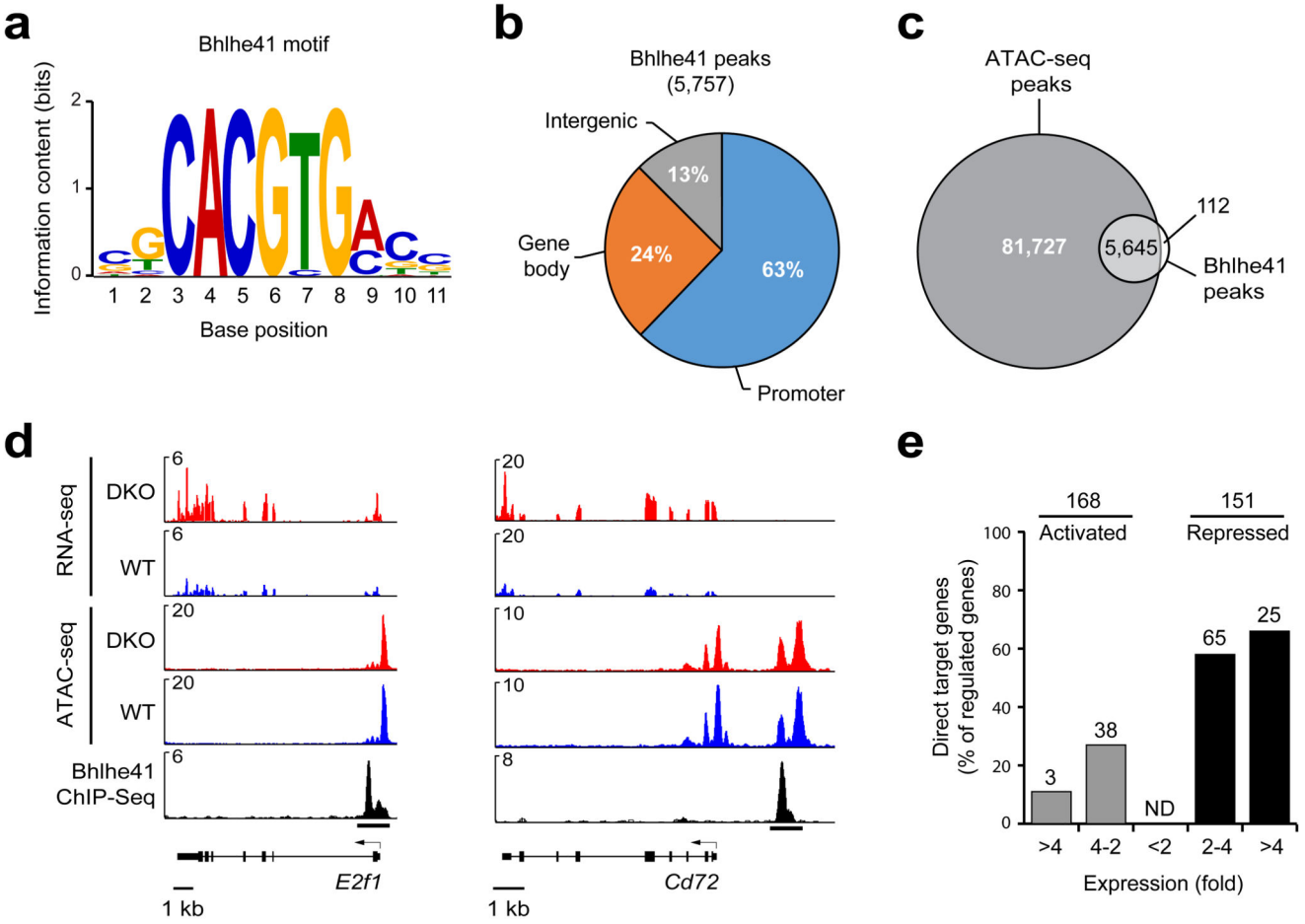


**Figure 5. Identification of regulated Bhlhe41 target genes in B-1a cells.**

(**a**) Consensus Bhlhe41-binding motif identified with an E-value of 1.3 x $10^{-120}$ by the *de novo* motif-discovery program MEME-ChIP. (**b**) Presence of Bhlhe41 peaks at the indicated gene regions. (**c**) Overlap of Bhlhe41 peaks with open chromatin regions, which were mapped by ATAC-seq39. (**d**) Presence of open chromatin (ATAC-seq) and RNA transcripts (RNA-seq) at the repressed Bhlhe41 target genes *E2f1* and *Cd72* in $V_H12/V\kappa4$ transgenic wild-type and DKO B-1a cells. Bhlhe41 binding was determined by ChIP-seq analysis of $V_H12/V\kappa4$ transgenic *Bhlhe41*$^{Tag/Tag}$ B-1a cells. (**e**) Identification of regulated Bhlhe41 target genes in $V_H12/V\kappa4$ transgenic B-1a cell. The number (above bars) and frequency (vertical axis) of Bhlhe41 target genes is shown together with the indicated differences in mRNA expression (horizontal axis) in $V_H12/V\kappa4$ transgenic DKO B-1a cells relative to their expression in $V_H12/V\kappa4$ transgenic wild-type B-1a cells. The 168 activated and 151 repressed genes (without considering Bhlhe41 binding) were selected for an adjusted *P* value of < 0.05 and a TPM value (transcripts per million) of > 5 in one of the two cell types.

Europe PMC Funders Author Manuscripts

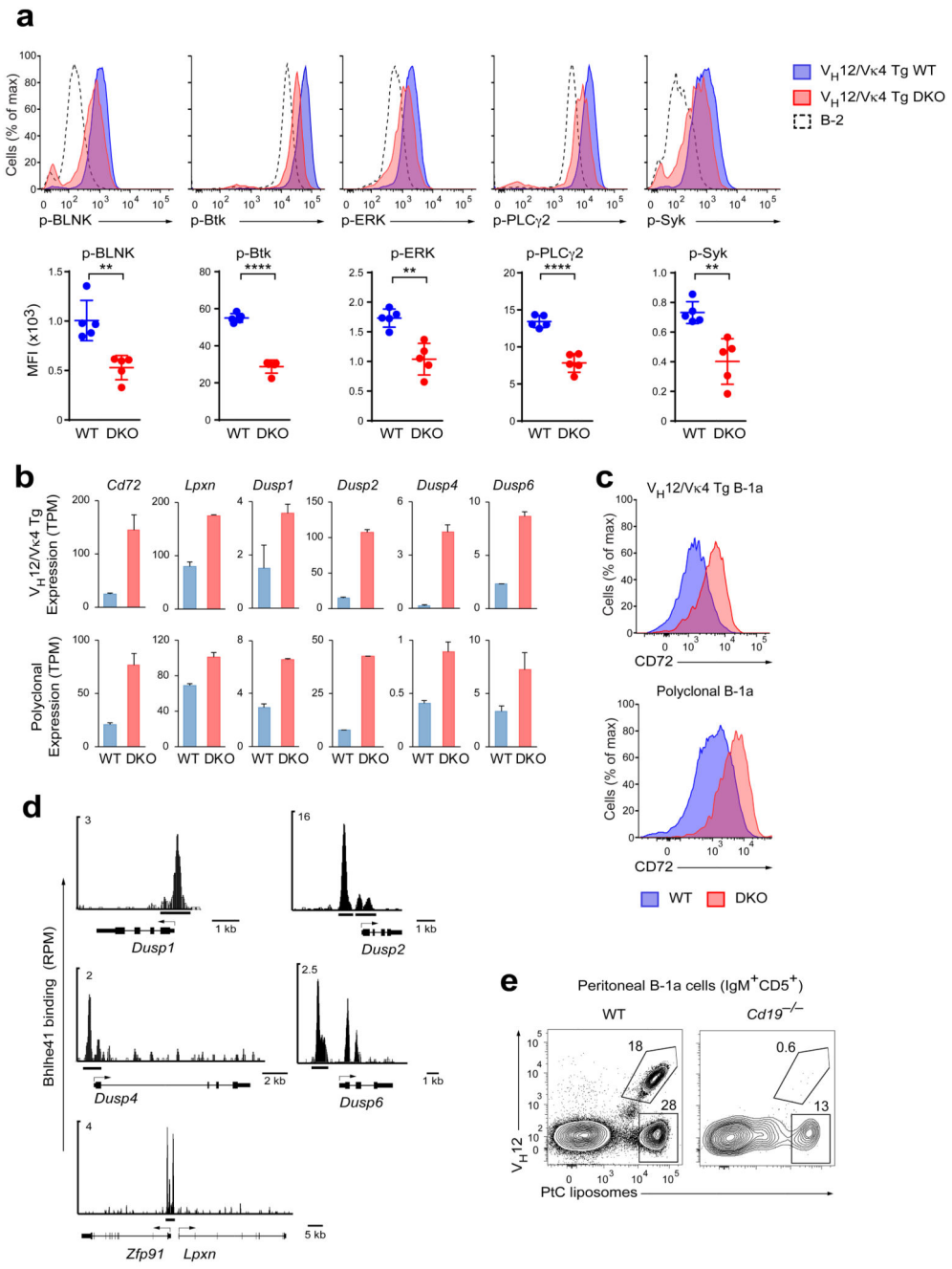


**Figure 6. Decreased BCR signaling in $V_H12/V\kappa4$ transgenic DKO B-1a cells.**

(**a**) The *ex vivo* phosphorylation status of the indicated BCR signaling components in $V_H12/V\kappa4$ transgenic wild-type and DKO B cells (10% chimeras) as well as in polyclonal B-2 cells was analyzed by flow cytometry. Representative FACS plots (top panels) and median fluorescence intensities (MFI) (bottom panels) are shown. Horizontal bars indicate mean value, and error bars represent SD. ** $P < 0.01$; **** $P < 0.0001$, as determined by the Student's *t*-test. Five chimeras were used per group. One representative result of two independent experiments is shown. (**b**) Expression of the indicated negative regulators of

BCR signaling in $V_H12/V\kappa4$ transgenic (top) and polyclonal (bottom) wild-type and DKO B-1a cells was determined by RNA-seq. TPM – transcripts per million. The data are from two independent RNA-seq experiments per cell type, and error bars indicate SEM. (**c**) Surface expression of CD72 on the indicated cell types. (**d**) Bhlhe41 binding (ChIP-seq) at the indicated gene loci that encode negative regulators of BCR signaling. (**e**) Binding of PtC-containing liposomes and expression of the $V_H12$ BCR by B-1a cells from wild-type and *Cd19*$^{-/-}$ mice. Eight wild-type mice and seven *Cd19*$^{-/-}$ mice were analyzed in three independent experiments. For statistical analysis see Supplementary Fig. 6d.



Europe PMC Funders Author Manuscripts

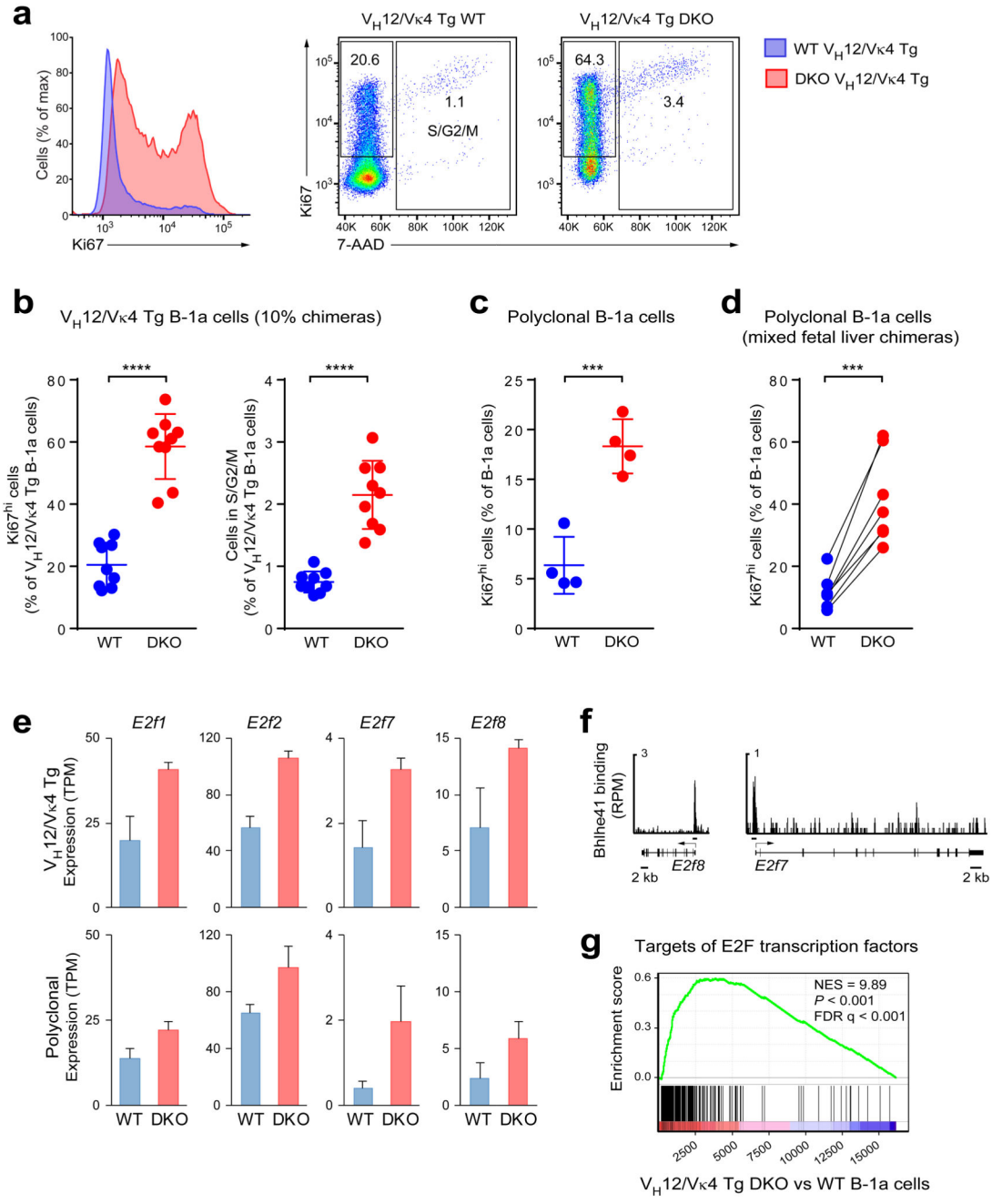


**Figure 7. DKO B-1a cells exhibit increased proliferation.**

(**a**) Anti-Ki67 and 7-AAD staining of fixed and permeabilized peritoneal B cells from $V_H12/V\kappa4$ transgenic wild-type and DKO mice. Histograms of Ki67 expression (left) and dot plots showing Ki67 and 7-AAD staining (right) are shown. A representative result of two independent experiments is shown. (**b**) Quantification of $Ki67^{hi}$ B cells and B cells in the S/G2/M phases of the cell cycle in an experiment performed with 10% chimeras. Horizontal bars indicate mean value, and error bars represent SD. **** $P < 0.0001$, Student's *t*-test. Nine chimeric mice were analyzed. One representative result of three independent




Europe PMC Funders Author Manuscripts

experiments is shown. (**c**) Quantification of peritoneal Ki67$^{hi}$ B-1a cells in non-transgenic wild-type and DKO mice. *** $P < 0.001$, Student's *t*-test. Four mice for each genotype were analyzed. One representative result of two independent experiments is shown. (**d**) Similar analysis of peritoneal B-1a cells from mixed fetal liver chimeras with non-transgenic wild-type and DKO cells (generated as described in the legend of Fig. 1f). Six chimeric mice were analyzed in one experiment. *** $P < 0.001$; Paired Student's *t*-test. (**e**) Expression of the genes encoding the indicated E2F transcription factors in $V_H12/V\kappa4$ transgenic (top) and polyclonal (bottom) wild-type and DKO B-1a cells was determined by RNA-seq. TPM – transcripts per million. The data are from two independent RNA-seq experiments per cell type, and error bars indicate SEM. (**f**) Bhlhe41 binding (ChIP-seq) at the *E2f7* and *E2f8* loci. (**g**) Gene set enrichment analysis (GSEA) of E2F target genes (gene set "Hallmark_E2F_Targets"; MSigDB) as compared to the ranked log2-fold gene expression changes between $V_H12/V\kappa4$ transgenic DKO and wild-type B-1a cells.

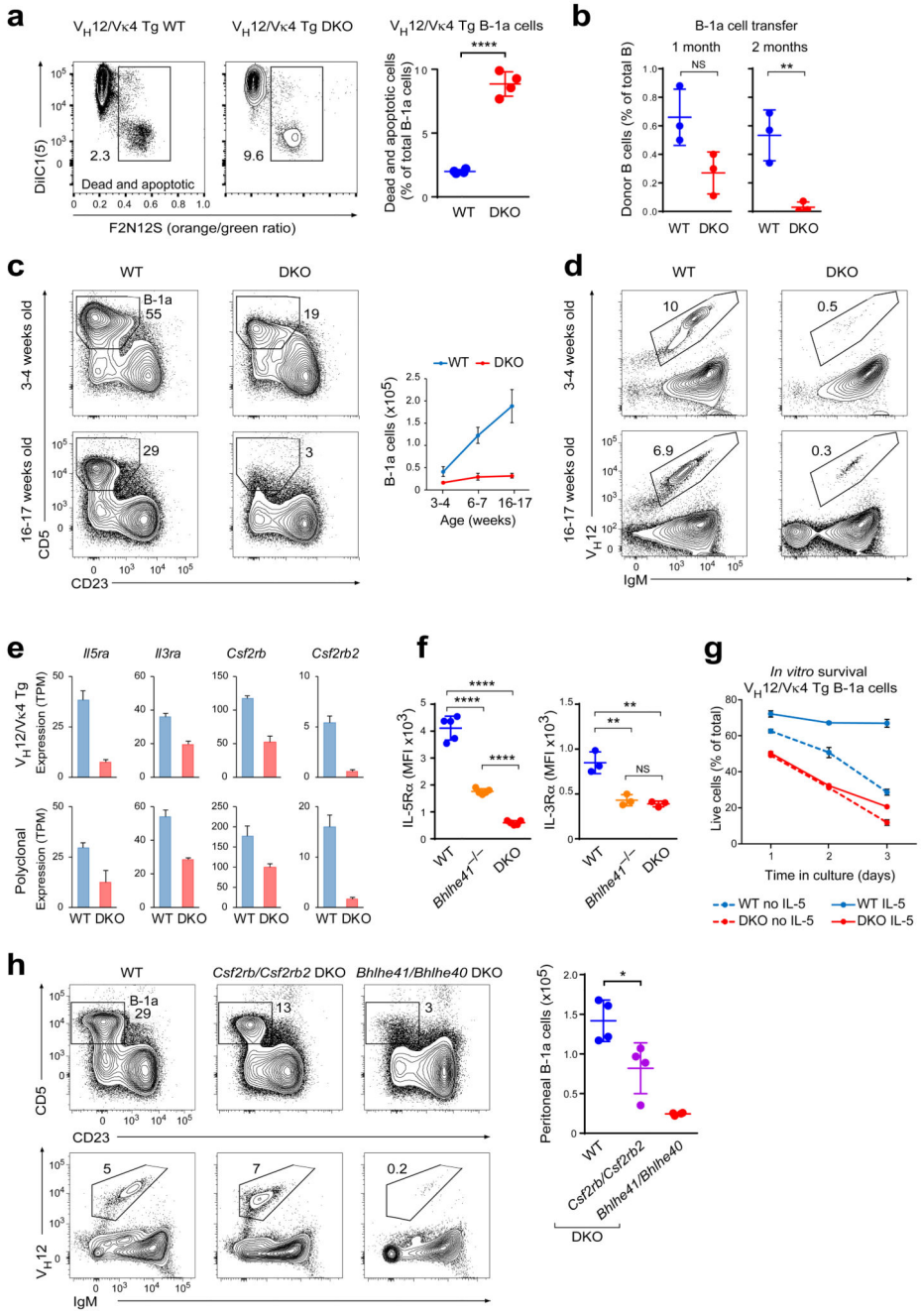


**Figure 8. Bhlhe41 and Bhlhe40 regulate B-1a cell self-renewal.**

(**a**) *Ex vivo* cell death of $V_H12/V\kappa4$ transgenic wild-type and DKO B cells (10% chimeras) was determined by loss of plasma membrane asymmetry (F2N12S ratiometric die staining) and loss of mitochondrial membrane potential (DiIC1(5) staining). Representative flow cytometry plots (left) and the quantification of dead and apoptotic cells (right) are shown. Horizontal bars indicate mean value, and error bars show SD. **** $P < 0.0001$, Student's *t*-test. Four chimeric mice were analyzed for each genotype. One representative result of two independent experiments is shown. (**b**) Equal numbers ($10^5$ cells) of sorted

$CD19^+CD5^+CD23^-$ B-1a cells from wild-type and DKO mice (CD45.2) were transferred intraperitoneally into sublethally irradiated wild-type recipients (CD45.1). The frequency of donor B cells ($CD19^+CD45.1^-CD45.2^+$) among total peritoneal $CD19^+$ B cells is shown for recipients analyzed at the indicated time after transfer. Three recipients were analyzed per group at each time point. Horizontal bars indicate mean value, and error bars show SD. NS $P > 0.05$; ** $P < 0.01$ as determined by the Student's *t*-test. Horizontal bars indicate mean value, and error bars show SD. One representative result of two independent experiments is shown. (**c**) The frequencies and absolute numbers of peritoneal B-1a cells were analyzed by flow cytometry in wild-type and DKO mice at the indicated age. Representative plots gated on peritoneal $CD19^+$ cells (left) and the quantification of B-1a cells (right) are shown for one experiment with 4 mice being analyzed per each group. Error bars indicate SD. (**d**) Representative flow cytometry plots showing IgM and $V_H12$ expression on peritoneal B-1 cell from mice at the indicated age. (**e**) Expression of the genes encoding the indicated α- and β-chains of the IL-5, IL-3 and GM-CSF receptor family in $V_H12/V\kappa4$ transgenic (top) and polyclonal (bottom) wild-type and DKO B-1a cells, as determined by RNA-seq. TPM – transcripts per million. The data are from two independent RNA-seq experiments per cell type, and error bars indicate SEM. (**f**) Quantification of surface IL-5Rα and IL-3Rα expression on polyclonal B-1a cells of the indicated genotypes. Horizontal bars indicate mean value, error bars represent SD. ** $P < 0.01$; **** $P < 0.0001$, Student's *t*-test. Five (IL-5Rα) and three (IL-3Rα) mice were analyzed per genotype. MFI – median fluorescence intensity. One representative result of two (IL-3Rα) and four (IL-5Rα) independent experiments is shown, respectively. (**g**) Peritoneal $V_H12/V\kappa4$ transgenic B-1a cells from bone marrow chimeras were sorted and incubated with or without IL-5 (10 ng/ml). Cultured cells were stained with 7-AAD at the indicated time points. The frequency of live cells (7-AAD-negative) at each time point is plotted. Three mice were analyzed per genotype. Error bars represent SD. One representative result of two independent experiments is shown. (**h**) Frequency and number of peritoneal B-1a cells and $V_H12^+$ B-1 cells in five-month-old wild-type, *Csf2rb/Csf2rb2* mutant and *Bhlhe41/Bhlhe40* mutant mice. Horizontal bars indicate mean value, error bars represent SD. * $P < 0.05$; Student's *t*-test. Four mice were analyzed per genotype. One representative result of three independent experiments is shown.